Oral Presentation

16 SEM-micro-photogrammetry and stereo reconstruction on the Tescan Amber X electron microscope
Evgenii Modin[1], Andrey Chuvilin
[1]CIC NanoGune BRTA, San Sebastian, Spain
140 Using secondary electron electron beam induced current for characterization of nanoparticle morphologies
Dr. Evgenii Vlasov[1,2], Mr. Wouter Heyvaert[1,2], Dr. Robin Girod[1,2], Prof. Luis M. Liz-Marzán[3], Prof. Johan Verbeeck[1,2], Prof. Sara Bals[1,2]
[1]EMAT, University of Antwerp, Antwerp, Belgium, [2]NANOlab Center of Excellence, University of Antwerp, Antwerp, Belgium, [3]CIC biomaGUNE, Basque Research and Technology Alliance (BRTA), Donostia-San Sebastián, Spain
144 Three-dimensional fivefold misfit in multiply twinned particles at atomic level
Assistant Professor Jihan Zhou[1], Ms. Zhen Sun[1], Mr Yao Zhang[1], Mr Zezhou Li[1], Mr Zhiheng Xie[1], Mr. Yiheng Dai[1], Dr Colin Ophus[2]
[1]Beijing National Laboratory for Molecular Sciences, Center for Integrated Spectroscopy, College of Chemistry and Molecular Engineering,Peking University, Beijing, China, [2]National Center for Electron Microscopy, Molecular Foundry, Lawrence Berkeley National Laboratory, Berkeley, USA
431 The geometry of STEM tomography
Matthew Weyland[1]
[1]Monash Centre for Electron Microscopy, Monash University, , Australia, [2]Department of Materials Science and Engineering, Monash University, , Australia
496 Multi-scale electron tomography in liquid state and its application to the study of beam-sensitive nanomaterials
Dr. Louis Marie Lebas[1], Dr Lucian Roiban[1], Dr. Victor Trillaud[1], Dr. Mimoun Aouine[2], Professor Karine Masenelli-Varlot[1]
[1]INSA Lyon, Université Claude Bernard Lyon 1, CNRS, MATEIS, UMR5510, Villeurbanne, France, [2]IRCELYON, UMR 5256 CNRS & Université Lyon 1, 2 avenue Albert Einstein, F-69626 , Villeurbanne, France
608 Reliable tomographic reconstructions of (sub)-nm gaps in plasmonic gold dimers for correlation to optical properties
Francesca Scalerandi[1], Dr Wiebke Albrecht[1], Dr Alexander Skorikov[2], Dr Nathalie Claes[3], prof Sara Bals[3]
[1]AMOLF, Amsterdam, The Netherlands, [2]CWI, Amsterdam, The Netherlands, [3]EMAT, Antwerp, Belgium

Poster Presentation

102 Achieving atomic precision 3D reconstructions through Bayesian genetic optimisation
Mr. Tom Stoops[1,2], Dr. Annick De Backer[1,2], Prof. Dr. Sandra Van Aert[1,2]
[1]EMAT, University of Antwerp, , Belgium, [2]NANOlab Center of Excellence, University of Antwerp, , Belgium
128 Unraveling the True 3D Structure of Colloidal Assemblies by Liquid Cell Electron Tomography
Daniel Arenas Esteban[1], Dr. Da Wang[1,2], Dr. Ajinkya Kadu[1,3], Mr. Noa Olluyn[1], Dr. Ana Sanchez Iglesias[4,5,6], Dr. Alejandro Gomez-Perez[7], Dr. Jesús Gonzalez Casablanca[8], Dr. Stavros Nicolopoulos[7], Prof. Luis M. Liz-Marzán[4,5,9,10], Prof. Sara Bals[1]
[1]Electron Microscopy for Materials Science (EMAT) and NANOlab Center of Excellence, University of Antwerp, Antwerp, Belgium, [2]Guangdong Provincial Key Laboratory of Optical Information Materials and Technology, South China Normal University, Guangzhou, China, [3]Centrum Wiskunde &

Informatica (CWI), Amsterdam, The Netherlands, [4]CIC biomaGUNE, Donostia-San Sebastián, Spain, [5]Centro de Investigación Biomédica en Red, Bioingeniería, Biomateriales y Nanomedicina, CIBER-BBN, Donostia-San Sebastián, Spain, [6]Centro de Física de Materiales CSIC-UPV/EHU, Donostia-San Sebastián, Spain, [7]NanoMEGAS SRPL, Brussels, Belgium, [8]Universidad Rey Juan Carlos, Centro de Apoyo Tecnológico, Madrid, Spain, [9]Ikerbasque, Basque Foundation for Science, Bilbao, Spain, [10]Cinbio, Universidade de Vigo, Vigo, Spain

184 Multi-scale characterization of vitamin B2 (riboflavin) supplements using X-ray Microscopy, SEM, and automated phase analyses

Ria Mitchell[1], Dr Darragh Murnane[2], Mr Andy Holwell[1]
[1]Carl Zeiss Microscopy Ltd, Cambourne, UK, [2]University of Hertfordshire, Hatfield, UK

426 Quantification of chirality from electron tomography data

Robin Girod[1], Dr. Mikhail Mychinko[1], Kyle Van Gordon[2], Bing Ni[3,4], Francisco Bevilacqua[2], Luis Liz-Marzan[2,5,6,7], Sara Bals[1]
[1]EMAT and NANOlab Center of Excellence, University of Antwerp, Groenenborgerlaan 171, Antwerp B-2020, Belgium, , , [2]CIC biomaGUNE, Basque Research and Technology Alliance (BRTA), 20014 Donostia-San Sebastián, Spain, , , [3]Physical Chemistry, University of Konstanz, Universitätsstrasse 10, 78457 Konstanz, Germany, , , [4]Present adress: Department of Chemical Engineering, University of Michigan, Ann Arbor, MI USA, , , [5]Centro de Investigación Biomédica en Red, Bioingeniería, Biomateriales y Nanomedicina (CIBER-BBN), 20014 Donostia-San Sebastián, Spain, , , [6]Ikerbasque, Basque Foundation for Science, 48009 Bilbao, Spain, , , [7]CINBIO, University of Vigo, 36310 Vigo, Spain, ,

588 Image fusion for 3D reconstruction of SEM images

Dr Turkka Salminen[1], Dr Lucio Azzari[1]
[1]Tampere Microscopy Center, Tampere University, Tampere, Finland

596 Real-time undersampling optimization during electron tomography of beam-sensitive samples using golden ratio scanning and RECAST3D

Mr. Timothy Craig[1], Dr. Ajinkya Kadu[1], Prof. Dr. Kees Batenburg[2], Prof. Dr. Sara Bals[1]
[1]Electron Microscopy for Materials Science and NANOlab Center of Excellence University of Antwerp, Antwerp, Belgium, [2]Leiden Institute of Advanced Computer Science, Leiden University, Leiden, The Netherlands

629 Deep image prior for limited-angle electron tomography

Dr Zineb SAGHI[1], Laure Guetaz[2], Thomas David[2], Philippe Ciuciu[3], Zineb Saghi[1]
[1]Univ. Grenoble Alpes, CEA, Leti, F-38000, Grenoble, France, [2]Univ. Grenoble Alpes, CEA, Liten, F-38000, Grenoble, France, [3]Univ. Paris Saclay, CEA-NeuroSpin, INRIA, Parietal, Gif-sur-Yvette, France

708 Improving electron tomography of mesoporous silica structures by Ga intrusion

Thomas Przybilla[1], Johannes Böhmer[1], Alexander Kichigin[1], Moritz Buwen[1], Alexander Götz[1], Dominik Drobek[1], Jakob Söllner[2], Matthias Thommes[2], Benjamin Apeleo Zubiri[1], Erdmann Spiecker[1]
[1]Institute of Micro- and Nanostructure Research (IMN) & Center for Nanoanalysis and Electron Microscopy (CENEM), Department of Materials Science and Engineering, Friedrich-Alexander-Universität Erlangen-Nürnberg, Erlangen, Germany, [2]Institute of Separation Science and Technology, Department of Chemical and Biological Engineering, Friedrich-Alexander-Universität Erlangen-Nürnberg, Erlangen, Germany

715 Momentum-resolved STEM Tomography of Gold-Silver core-shell Nanoparticles

Sebastian Sturm[1], Dr. Felizitas Kirner[2], Prof. Dr. Elena Sturm[2], Prof. Dr. Knut Müller-Caspary[1]
[1]Ludwig-Maximilians-Universität München, Department of Chemistry, Munich, Germany, [2]Ludwig-Maximilians-Universität München, Department of Earth and Environmental Sciences, Munich, Germany

743 Deep Learning assisted X-ray Microscopy Characterization of Nickel based Metal Matrix composite reinforced with TiC

Dr. Kaushik Yanamandra[1], Dr. Hrishikesh Bale[1], Dr. Rajarshi Banerjee[2], Ria Mitchell[1]

[1]Carl Zeiss Research Microscopy Solutions, Dublin, United States of America, [2]Materials Science and Engineering, University of North Texas, Denton, United States of America

843 Advanced acquisition strategies for lab-based diffraction contrast tomography

Florian Bachmann[1], Jun Sun[1], Jette Oddershede[1], Erik Lauridsen[1]
[1]Xnovo Technology ApS, Køge, Denmark

860 4D-STEM Optical Sectioning of Dopants in Diamond

Mr. Aidan Horne[1], Mr. Jacob Lewis[1], Mr. Emmanuel Tegegne[1], Dr. Peng Wang[1]
[1]University of Warwick, Coventry, United Kingdom

878 Understanding field evaporation sequences by in-situ correlative microscopy and simulation

Mohammed Ilhami[1], Prof. Williams Lefebvre[1], Prof. Francois Vurpillot[1]
[1]Groupe De Physique Des Matériaux, Saint Etienne Du Rouvray, France

894 Simulating iDPC tomography of CeO2 nanoparticles with experimentally realistic parameters and conditions

Miss Ella Kitching[1], Dr Thomas Slater[1]
[1]Cardiff Catalysis Institute, School of Chemistry, Cardiff University, Cardiff, United Kingdom

903 Complementary vEM approaches for ultrastructural changes during the development of D. melanogaster germline intercellular bridges

Dr Irina Kolotuev[1], Abigayle Elsbury[2], Caroline Kizilyaprak[1], Stephanie Pellegrino[2], Dr Lindsay Lewellyn[2]
[1]Faculté de Biologie et de Médecine, Université de Lausanne, Lausanne, Switzerland, [2]Department of Biological Sciences, Butler University, Indianapolis, USA

1071 Investigation of GaAs-based nanowire heterostructures using tomography based on STEM-HAADF tilt-series[1]

Richard Zell[1], Sebastian Sturm[1], Hyowon W. Jeong[2], Prof. Gregor Koblmüller[2], Prof. Knut Müller-Caspary[1]
[1]Ludwig-Maximilians-Universität, Munich, Germany, [2]Technical University of Munich, Munich, Germany

1098 In-Situ microscopy study on self-healing process of vitrimers

Tobias Krekeler[1], Siraphat Weerathaworn[2], Matthias Hemmleb[3], Volker Abetz[2], Martin Ritter[1]
[1]Hamburg University of Technology, Hamburg, Germany, [2]University of Hamburg, Hamburg, Germany, [3]point electronic GmbH, Halle (Saale), Germany

1140 Visualisation of lepidopteran silk gland morphology using X-ray micro-computed tomography scanning technique

Mgr. Šárka Podlahová[1,2], Mgr., Ph.D. Gabriela Krejčová[1], Mgr., Ph.D. Hana Sehadová[1,2]
[1]University of South Bohemia in České Budějovice, Faculty of Science, České Budějovice, Czech Republic, [2]Biology Centre of the Czech Academy of Sciences, Institute of Entomology, Ceske Budejovice, Czech Republic

16

SEM-micro-photogrammetry and stereo reconstruction on the Tescan Amber X electron microscope

Evgenii Modin[1], Andrey Chuvilin
[1]CIC NanoGune BRTA, San Sebastian, Spain

IM-01, Lecture Theater 1, august 26, 2024, 14:00 - 16:00

Three-dimensional imaging techniques are widely demanded in various fields including science, medicine, engineering, architecture, and art [1,2]. Combining these techniques with scanning electron microscopy capabilities yields interesting results and extends the capabilities of scanning electron microscopy beyond two-dimensional imaging, opening up new applications.
In our lab, we are exploring the potential of scanning electron microscopy to investigate the three-dimensional surface morphology of a variety of complex objects, from the surface of construction materials to the spatial geometry of micromachined parts and marine organisms.
One of the methods of three-dimensional reconstruction is photogrammetry, which has been actively used in recent decades, especially in the field of geodesy. Another method under study is stereoscopy, which uses a sophisticated algorithm to calculate the surface profile from a pair of images acquired at different tilt angles.
We use automatic data acquisition on the Tescan Amber X instrument thanks to the support of Python scripts (Shark SEM Advanced). It is shown that even quite large objects are suitable for correct scanning without the need for image stitching. Further, the Structure from Motion photogrammetry methodology implemented in AliceVision Meshroom and AgiSoft Metashape software packages is used to calculate three-dimensional models. However, it should be noted that this method requires not only an accurate dataset, but also significant computational resources. Ongoing work in this area explores the use of neural network-based neural radiance fields (NERFs) for on-the-fly reconstruction [3].
The stereoscopic method reconstructs the surface profile from two photographs taken at different sample angles, typically ±5 degrees or close to it. Unlike the implemented algorithms available in the literature and well-known commercial packages, our software can use gigapixel images, allowing the characterization of millimeter-scale regions with nanometer resolution and thus meeting and exceeding the ISO 4287-1997 standard in surface topography characterization.

1. Drofova, I.; Guo, W.; Wang, H.; Adamek, M. Use of Scanning Devices for Object 3D Reconstruction by Photogrammetry and Visualization in Virtual Reality. Bull. Electr. Eng. Inform. 2023, 12, 868–881.
2. Scianna, A.; La Guardia, M. Survey and Photogrammetric Restitution of Monumental Complexes: Issues and Solutions—The Case of the Manfredonic Castle of Mussomeli. Heritage 2019, 2, 774–786.
3. Pepe, M.; Alfio, V.S.; Costantino, D. Assessment of 3D Model for Photogrammetric Purposes Using AI Tools Based on NeRF Algorithm. Heritage 2023, 6, 5719-5731.

Keywords:

3d, surface reconstruction, photogrammetry

140

Using secondary electron electron beam induced current for characterization of nanoparticle morphologies

Dr. Evgenii Vlasov[1,2], Mr. Wouter Heyvaert[1,2], Dr. Robin Girod[1,2], Prof. Luis M. Liz-Marzán[3], Prof. Johan Verbeeck[1,2], Prof. Sara Bals[1,2]
[1]EMAT, University of Antwerp, Antwerp, Belgium, [2]NANOlab Center of Excellence, University of Antwerp, Antwerp, Belgium, [3]CIC biomaGUNE, Basque Research and Technology Alliance (BRTA), Donostia-San Sebastián, Spain

IM-01, Lecture Theater 1, august 26, 2024, 14:00 - 16:00

Background incl. aims
Electron tomography (ET) is an indispensable tool for determining the three-dimensional (3D) structure of nanomaterials in (scanning) transmission electron microscopy ((S)TEM). ET enables 3D characterization of a variety of nanomaterials across different fields, including life sciences, chemistry, solid-state physics, and materials science down to atomic resolution. However, the acquisition of a conventional tilt series for ET is a time-consuming process and thus cannot capture fast transformations of materials in realistic conditions. Moreover, only a limited number of nanoparticles (NPs) can be investigated, hampering a general understanding of the average properties of the ensemble. Therefore, alternative characterization techniques that allow for high-resolution characterization of the surface structure without the need to acquire a full tilt series in ET are required which would enable a more time-efficient investigation with better statistical value. Here we propose surface-sensitive secondary electron (SE) imaging in STEM employed using a modification of electron beam-induced current (EBIC) setup as an alternative surpassing electron tomography.
Methods
SEEBIC and ET experiments were performed using an aberration-corrected Thermo Fisher Themis Z TEM operated at an acceleration voltage in a range of 60-200 kV. A custom-made transimpedance amplifier with a total gain of 2 GV/A and bandwidth of 8 kHz, electrically connected to the sample via a DENSsolutions Wildfire holder, was used to convert the SEEBIC signal into a voltage signal digitized by the Attollight OUDS II scan engine. No image filtering was applied during post-processing. ET data were acquired over a tilt range of ±72° with tilt increments of 3°. Reconstructions of the tilt series were performed using the SIRT algorithm implemented in ASTRA Toolbox 1.90 for MATLAB 2022b. Scanning electron microscopy (SEM) images were obtained using Thermo Fisher Helios Nanolab 650 with nominal spatial resolution down to 0.8 nm operated at an acceleration voltage of 5 kV.
Results
We have shown that both general morphology and side faceting of the NPs can be directly observed from SEEBIC images which is less obvious from conventional STEM micrographs. SEEBIC imaging enables a gain of up to 2 orders of magnitude in data collection efficiency in comparison to conventional ET while providing necessary topographical information. The superior spatial resolution compared to SEM was demonstrated. It was shown that even though SEEBIC requires to use of high primary electron beam currents, the optimization of experimental parameters allows for the reduction of the accumulated electron dose rendering SEEBIC equally or even more dose-efficient than ET. Finally, we describe the contrast artefacts arising in SEEBIC images and discuss their origin. Next, it was shown that direct access to surface morphology obtainable on the order of minutes opens up the possibility of using SEEBIC for high-throughput analysis of the helical morphology of chiral Au nanorods (NRs). The workflow to automatically quantify the helical morphology based on SEEBIC images and a dedicated image quantification procedure was developed and used to calculate the helicity function of the NP ensembles. We have shown that this approach overcomes the limitation of poor statistics obtained by ET, which is limited to analyzing only a few particles per

sample batch. Helicity function analysis revealed a significant polydispersity at the level of surface features. We found that the average helicity values, calculated for hundreds of NRs per sample batch were in good agreement with the optical properties of the sample, confirming that helicity measurements enable linking the nanoscale morphology with the chiroptical handedness.

Conclusion

We have demonstrated that SEEBIC can be considered an attractive approach for the characterization of NP morphologies with shorter acquisition and processing times in comparison to ET and superior resolution in comparison to SEM. It was shown that the helical morphology of chiral Au NRs, with significant polydispersity at the level of surface features can be efficiently quantified using high-throughput SEEBIC measurements.

This work was supported by European Research Council (ERC Consolidator Grant 815128, REALNANO).

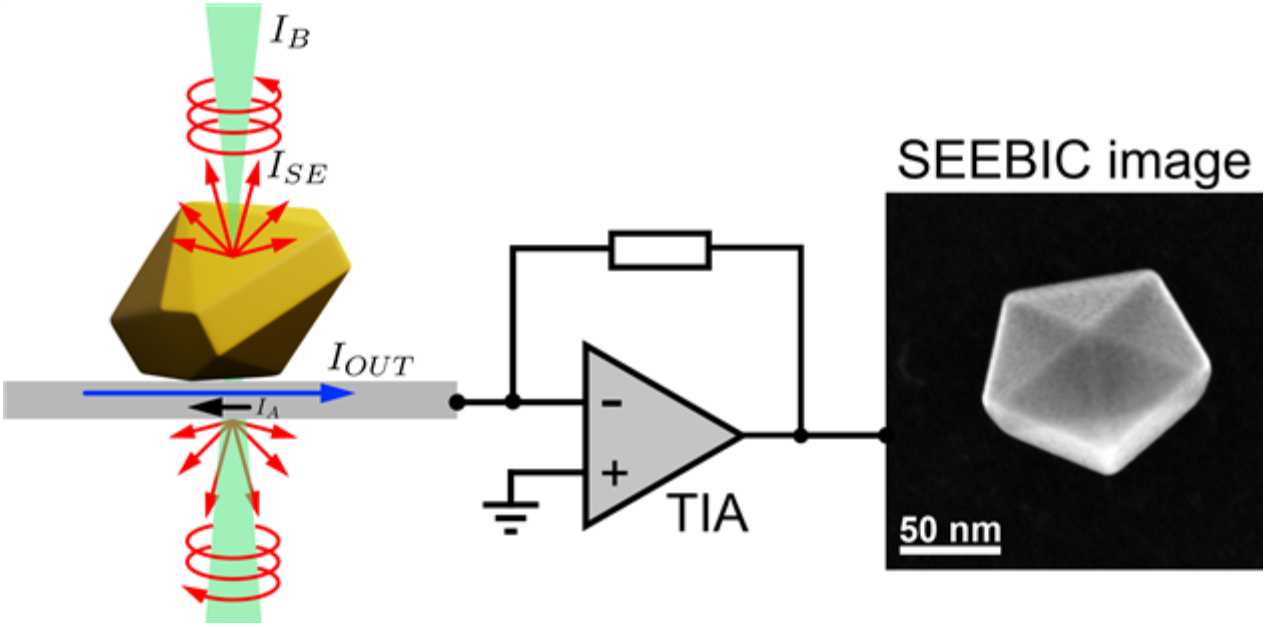

Keywords:

STEM, electron tomography, SE imaging

Reference:

[1] W. Hubbard, et al, Phys. Rev. Appl. 2018, 10, 044066.
[2] E. Vlasov et al, ACS Mater. Lett. 2023, 5, 1916.

144

Three-dimensional fivefold misfit in multiply twinned particles at atomic level

Assistant Professor Jihan Zhou[1], Ms. Zhen Sun[1], Mr Yao Zhang[1], Mr Zezhou Li[1], Mr Zhiheng Xie[1], Mr. Yiheng Dai[1], Dr Colin Ophus[2]
[1]Beijing National Laboratory for Molecular Sciences, Center for Integrated Spectroscopy, College of Chemistry and Molecular Engineering,Peking University, Beijing, China, [2]National Center for Electron Microscopy, Molecular Foundry, Lawrence Berkeley National Laboratory, Berkeley, USA

IM-01, Lecture Theater 1, august 26, 2024, 14:00 - 16:00

Background incl. aims
Fivefold symmetry is mysterious in crystallography because it lacks translational invariance and periodic structures. We cannot fill two-dimensional (2D) planes with regular pentagons or make an icosahedron with regular tetrahedra (Figure 1a-b). Multiply twinned particles (MTPs) have attracted attention since their discovery because of their excellent optical and catalytic properties, crystallographically forbidden fivefold symmetry and associated lattice misfit strain. Icosahedral MTPs composed of fivefold twinned tetrahedra have broad applications and the researchers have observed from 2D perspective for decades [1-7]. Electron tomography offers a method to image internal distortions and visualize successive twinning in three-dimensional (3D) [8-9]. However, the atomic misfit, the associated strain relief mechanism, and the bridging solid-angles in icosahedral MTPs are not yet quantitatively understood in 3D, primarily due to a lack of experimentally obtained 3D atomic structures of MTPs.
Methods
Gold MTPs, coated with a thin shell of palladium, and Pd@Pt core-shell MTPs were synthesized and deposited on thin Si3N4 film for high resolution imaging. We employed atomic resolution electron tomography to determine the 3D atomic coordinates of the MTPs. In short, the tomographic tilt series were acquired with aberration-corrected STEM in annular dark-field mode. After drift correction and denoising, we reconstructed the tomographic tilt series using the real space iterative reconstruction (RESIRE) algorithm; we then traced and classified the 3D atomic coordinates and chemical species.
Results
Here, we determined the 3D atomic structures of Janus icosahedral nanoparticles using atomic resolution electron tomography. A geometrically fivefold face (C5 side) consistently corresponds to a less ordered face (C5’ side) like two hemispheres (Figure 1c-d). We found that the 3D angular deficiency is compensated by insertion of edge dislocations and amorphization of several tetrahedra. The disordered amorphous domain with the largest solid angle is 14.6° larger than the ideal fcc domain, relaxing a large amount of strain and filling the largest angular defects (Figure 1e-h). Edge dislocations fill the angular deficiency near the axis. Our research has unveiled, for the first time, how the spatial gap of the icosahedron is compensated at the 3D atomic scale and provide a completely new insight on atomistic models for the modelling of formation mechanisms of fivefold and icosahedral twinned structures by molecular dynamics as well as computer simulations of lattice distortions and defects..
Conclusion
The novel physical insights are 1). We clearly show that the 3D angular deficiency is compensated by insertion of edge dislocations and amorphization of several tetrahedra instead of homogeneous dilatation in all the twenty tetrahedra. 2) Many structural characteristics of the icosahedral MTPs are divided into two groups spatially distributed in two hemispheres of the MTPs, such as the bond orientation order parameters, solid angle, and the number of atoms. The twelve fivefold axes are not uniformly distorted; edge dislocations are preferably distributed in one side of the particle. Our

observations provide a completely new insight on atomistic models for the modelling of formation mechanisms of fivefold and icosahedral twinned structures by molecular dynamics as well as computer simulations of lattice distortions and defects.

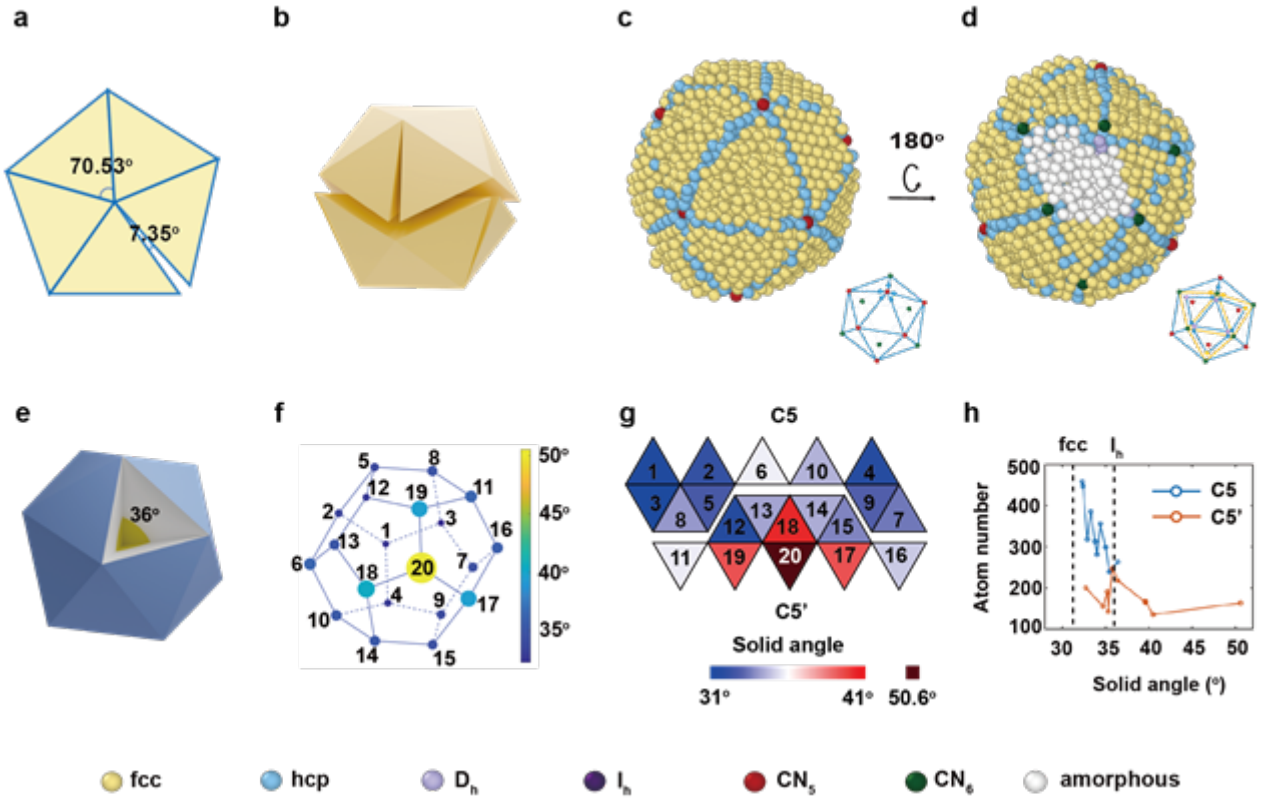

Keywords:

Fivefold, multiply twinned particles, icosahedron

Reference:

[1] S. Ino, et al. J. Phys. Soc. Jpn. 27, (1969), 941–953.
[2] L. D. Marks, et al. Nature 282, (1979), 196–198.
[3] M. R. Langille, et al. Science 337, (2012), 954–957.
[4] M. Song, et al. Science 367, (2020), 40–45.
[5] Z. Li, et al. Nat. Commun. 14, (2023), 2934.

431

The geometry of STEM tomography

Matthew Weyland[1]
[1]Monash Centre for Electron Microscopy, Monash University, , Australia, [2]Department of Materials Science and Engineering, Monash University, , Australia

IM-01, Lecture Theater 1, august 26, 2024, 14:00 - 16:00

Electron tomography (ET) by scanning transmission electron microscopy (STEM) [1], is a mature technique which has become part of the standard repository of tools available to electron microscopists in the physical sciences [2]. The acquisition of datasets is often carried out using commercially purchased automated acquisition tools, available from a number of microscope [3], accessory manufacturers or freeware solutions [4]. These automated tools save time, minimise dose, reduce the potential for error and prevent the operator dying from boredom. Whichever package is used for the acquisition they tend to follow a set approach, codified during the development of STEM tomography in the early 2000's [1]. This, while it works, has a number of problematic characteristics that have never been addressed in subsequent studies. One of these problems is the mismatch between the relative geometries of the STEM acquisition and that which is ideal for tomographic reconstruction. This is a consequence of choosing the scan rotation to place the fast scan direction parallel to the tilt axis; usually to allow the use of dynamic focussing. This choice just happens to maximise the degradation of the quality of the data due to specimen drift. The nature of this mismatch will be explored and demonstrated using both theory and experiment. The theory will be demonstrated with phantoms and the experiments will apply "forced" drift to accentuate the issues. A number of different solutions will be suggested and demonstrated. The potential for improved quality in reconstructions will be explored and discussed.

Keywords:

Tomography, STEM

Reference:

[1] Midgely, P.A and Weyland, M. Ultramicroscopy 96, p413 (2003)
[2] Hayashida, M. and Malac, M. Micron 91, p49 (2016)
[3] Kubel, C. et al, Microscopy & Microanalysis 11, p378 (2005)
[4] Schorb, M. et al, Nature Methods 16 (6), p471 (2019)

496

Multi-scale electron tomography in liquid state and its application to the study of beam-sensitive nanomaterials

Dr. Louis Marie Lebas[1], Dr Lucian Roiban[1], Dr. Victor Trillaud[1], Dr. Mimoun Aouine[2], Professor Karine Masenelli-Varlot[1]
[1]INSA Lyon, Université Claude Bernard Lyon 1, CNRS, MATEIS, UMR5510, Villeurbanne, France, [2]IRCELYON, UMR 5256 CNRS & Université Lyon 1, 2 avenue Albert Einstein, F-69626 , Villeurbanne, France

IM-01, Lecture Theater 1, august 26, 2024, 14:00 - 16:00

Background incl. aims

Electron tomography is a technique that allows 3D data analysis at the nanometer scale. In its early days, it was performed in high vacuum and only beam-resistant samples were analyzed due to its time-consuming nature. In the last decade, tremendous technical developments have been made to make tilt series acquisition faster and faster, and to make fast electron tomography compatible with environmental electron microscopy. [1,2]
Environmental electron tomography in gas, and even more so in liquid state, is very sensitive to the electron beam, so acquiring fast tilt series in STEM mode with a very low electron dose received by the sample is a real challenge even for the most experienced users. In this presentation the application of the M-SIS software, developed in our group, in the analysis of aluminum hydrogel suspended in liquid will be shown.

Methods

Al(OH)3 is an extremely beam sensitive sample, so care must be taken to avoid beam damage, especially when the sample is in a liquid state. An aqueous suspension of aluminum hydrogel was inserted into the ESEM in the liquid state, then dried and rehydrated in situ. At each hydrated state, a fast tilt series in STEM mode from -70° to +70° was recorded on the region of interest at low electron dose in order to preserve the sample. In addition, ETEM experiments were carried out without encapsulating the sample. A careful control of the sample temperature and the water vapor pressure enabled the 3D study of the hydrated material at nanometer scale and the pore size distribution was measured. The tilt series were recorded using the custom code M-SIS build in Python that is an automatic tool for electron tomography and can be installed on an ESEM and on an ETEM.[1-3]

Results

Three hydration states of Al(OH)3 were investigated in 3D by ESEM. It was found that the global volume of the sample does not change its structure during the dehydration-rehydration cycle. Its change in volume was measured to be about - 3.4 ± 1.3% during dehydration, followed by a + 1.2 ± 1.0% expansion during rehydration. The spatial resolution of the tomograms was about 10 nm and the total electron dose of each tomogram was between 1050 and 1250 e-nm-1.
In ETEM, tilt series could be acquired with 260 frames in 12 min, with a pixel size of 0.6 nm and a total electron dose of 16,000 e-nm-1. No significant change of the sample structure could be detected during acquisition. The pore size distribution in the hydrated state was found to vary from 5 to 30 nm (Figure 1).

Conclusion

Thanks to the development of the M-SIS software, we are now able to study beam-sensitive materials in liquid in 3D. Al(OH)3, an extremely beam-sensitive material, was analyzed in ESEM in 3D in different hydration states. The morphological changes were quantified with a spatial resolution of 10 nm. The pore size distribution in the hydrated sample was quantified with higher resolution in liquid using electron tomography in ETEM.

Figure 1: 3D model of Al(HO)3 in the initial state in liquid, then after dehydration and finally after rehydration. The yellow particles are Au particles used as fiducial model.

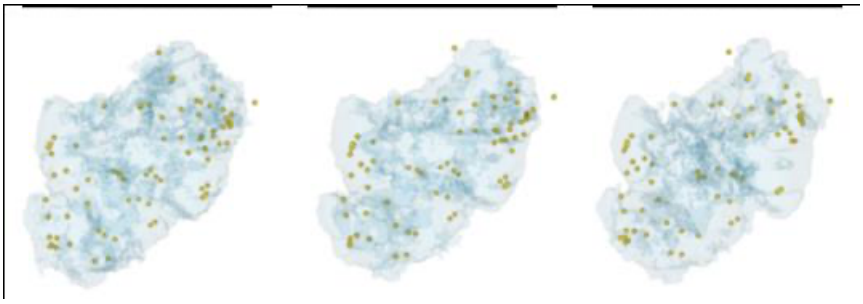

Keywords:

In-situ, liquide, beam sensitive, tomography

Reference:

[1] S. Koneti et al, Fast electron tomography: Applications to beam sensitive samples and in situ TEM or operando environmental TEM studies. Materials Characterization 151, 2019.
[2] X. Jiao et al, Electron tomography on latex particles suspended in water using environmental scanning electron microscopy, Micron, 2019, 117.
[3] the Consortium Lyon Saint-Etienne de Microscopie (CLYM) is acknowledged for microscope access, and ANR for funding (project ANR-20-CE92-0014-01).

608

Reliable tomographic reconstructions of (sub)-nm gaps in plasmonic gold dimers for correlation to optical properties

Francesca Scalerandi[1], Dr Wiebke Albrecht[1], Dr Alexander Skorikov[2], Dr Nathalie Claes[3], prof Sara Bals[3]
[1]AMOLF, Amsterdam, The Netherlands, [2]CWI, Amsterdam, The Netherlands, [3]EMAT, Antwerp, Belgium

IM-01, Lecture Theater 1, august 26, 2024, 14:00 - 16:00

Different decay paths govern plasmon damping. Among them, direct charge transfer has incredible potential in several applications from quantum optics to biosensing, but its exact mechanisms are still an open question [1][2][3]. We investigate the optical properties of plasmonic gold nanosphere-dimers separated by nanometer sized gaps towards the optimization of direct charge transfer. The dimers are synthetized with a molecular junction of conductive dithiol molecules in the gap. The optical response of metal nanoparticles is ruled by their exact three-dimensional morphology [1]. This is particularly critical for investigating charge transfer, which depends on the exact gap size. Different techniques are available to investigate the shape of nanomaterials. Among them, transmission electron microscopy (TEM) allows for atomic resolution. However, TEM images are 2D projections of 3D objects, resulting in the loss of valuable three-dimensional information. This loss can be especially detrimental for extracting quantitative information for non-symmetric structures or in case of objects that do not lie perfectly flat on the substrate. Three-dimensional information can be obtained by electron tomography (ET).

In this work, we begin by addressing the limitations of 2D high-angle annular dark-field scanning transmission electron microscopy (HAADF-STEM) and 3D ET, with particular focus on the gap reconstruction. We discuss the difficulties that emerge, both in 2D and 3D, when defining thresholds for extracting the quantitative morphology. We then combine experiments and simulations to address ET's challenges in reconstructing (sub)- nanometer gaps in gold dimers. We introduce a model for fitting sub-nanometer interparticle gaps. The proposed model is based on the convolution of a Gaussian function and a step function. Finally, the results are correlated with optical measurements. Optical properties are investigated using a homemade confocal dark-field spectroscopy setup and electron energy loss spectroscopy (EELS).

We start by highlighting the limitations of 2D STEM for gap reconstructions. Different experimental STEM images of the exact same dimer taken at different tilt angles resulted in different gap sizes and strongly varied with the chosen image threshold. By changing these two parameters, the gap size can vary between 0.1 nm and 2 nm. Such large differences in gap sizes have tremendous effects on the optical properties. As shown in Fig.1, even rather minor changes in morphology significantly impacted the optical properties of the system. The inaccuracy in determining the gap sizes from the 2D STEM images (Fig. 1b) made it also impossible to simulate the optical properties of the dimers. In Fig. 1c the scattering cross sections were simulated based on the 2D morphology information. For that, the STEM images were thresholded with the Otsu method to extrapolate the morphological parameters, which were then used as input for the optical simulations. The simulations were performed using the MATLAB toolbox MNPBEM[4]. In Fig.1c, the experimental and simulated scattering spectra of four different dimers are displayed. The discrepancies between simulated and experimental scattering spectra suggest that 2D STEM images alone are insufficient for retrieving the morphology of the dimers.
Even when moving to electron tomography, we observed that the choice of threshold remained critical for the final gap reconstruction. Therefore, we developed a model to fit the data and retrieve

the gap size without running into the thresholding problem. The proposed model is based on the convolution of a Gaussian function and a step function. The validity of the model was first investigated on simulations and them applied to fit experimental data.
We are currently working towards extending the convolutional model to analyse 2D STEM data by including the thickness-dependent HAADF-STEM intensity[5] in the fitting procedure. This will enable gap size extrapolation without relying on thresholding methods.

In conclusion, in this work we highlight the limitations of 2D imaging for retrieving the morphology of plasmonic particles. We then advocate the use of electron tomography to achieve a better reconstruction of the system morphology. We introduce a model tailored to fit experimental data from electron tomography and extrapolate nanogap sizes with one pixel accuracy. Finally, by correlating optical properties and morphology, we demonstrate the importance of this accurate three-dimensional reconstruction. Being able to accurately simulate the optical properties and experimentally correlate it to the exact morphology will finally allow us to design plasmonic systems with fine-tuned properties. This can be crucial for applications in catalysis, sensing and quantum optics.

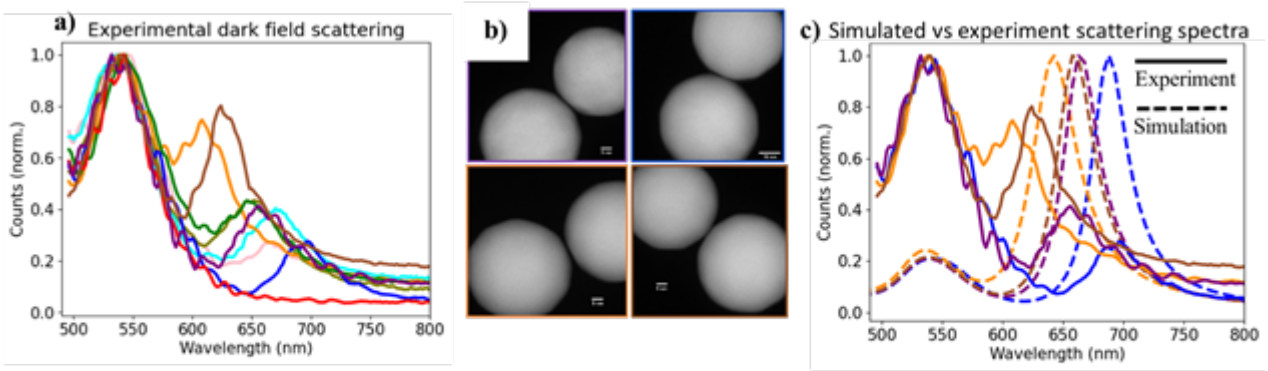

Fig. 1. **a)** Scattering spectra of various gold dimers. **b)** STEM images depicting some of the dimers corresponding to the scattering spectra shown in (a). **c)** Comparison between experimental and simulated scattering spectra for the same dimers.

Keywords:

plasmon, electron-tomography, correlation, optical properties

Reference:

[1] Wu, et al., “Efficient hot-electron transfer by a plasmon-induced interfacial charge-transfer transition”, Science, 2015, 349, 628–632
[2] Tan, Shu Fen et al., “Quantum plasmon resonances controlled by molecular tunnel junctions, Science vol. 343,6178 (2014): 1496-9
[3] Felix Benz et al., “Nanooptics of Molecular-Shunted Plasmonic Nanojunctions”, Nano Letters 2015 15 (1), 669-674
[4] U. Hohenester and A. Trügler, “MNPBEM – A Matlab toolbox for the simulation of plasmonic nanoparticles”, Comp. Phys. Commun. 183, 370 (2012).
[5] W. Van den Broek et al. “Correction of non-linear thickness effects in HAADF STEM electron tomography”, Ultramicroscopy, 2012, 0304-3991

102

Achieving atomic precision 3D reconstructions through Bayesian genetic optimisation

Mr. Tom Stoops[1,2], Dr. Annick De Backer[1,2], Prof. Dr. Sandra Van Aert[1,2]
[1]EMAT, University of Antwerp, , Belgium, [2]NANOlab Center of Excellence, University of Antwerp, , Belgium

Poster Group 1

Background incl. aims
Accurate and precise knowledge of the three-dimensional shape of nanoparticles is critical to understanding their unique properties. High-angle annular dark field scanning transmission electron microscopy (HAADF-STEM) provides a powerful tool for quantitative analysis, allowing the extraction of structural information through atom-counting, where the intensities generated by atomic columns in HAADF-STEM are analysed to count the number of atoms with single-atom precision.
However, reconstructing the 3D structure from these counting results remains challenging. Based on the counting results and the prior knowledge of the crystal structure, we can construct an initial guess of the nanoparticle by placing the columns symmetrically around a central plane. While this can serve as an initial guess, further refinement is imperative to make claims about the structure. In recent years several refinement procedures have been proposed. Molecular dynamics and Monte Carlo methods have been used for energy optimisation but may fall short of an accurate reconstruction by becoming trapped in local minima or deviating from experimental observations. A local minima search algorithm can scan the energy landscape for the best energy minimum but does not consider the finite precision of atom counting, which strongly contributes at lower electron doses.
Methods
The implementation of the Bayesian genetic algorithm can address these issues effectively. In contrast to molecular dynamics-based reconstruction methods, where each atom is individually considered, the Bayesian genetic algorithm is a holistic approach; it incorporates all knowledge obtained from the HAADF-STEM image. The column positions are fixed to the observed locations in the image, and the thickness variations are constrained by the known finite precision of the atom-counting analysis.
The initial guess for the three-dimensional structure created based on the atom-count results and prior knowledge of the crystal structure functions as a reference in the genetic sequence. By encoding parameters such as the height offset and thicknesses of columns with respect to the initial guess, we can describe any possible 3D structure generated by the columns in the observed image. The genetic algorithm will then utilise mutations and combinations of members to optimise a cost function. By generating large populations of candidate reconstructions with genetic variety, the algorithm can effectively scan the local energy landscape for an optimal solution which balances the energy minimisation and atom-counting probabilities.
However, genetic algorithms can become prohibitively computationally expensive for large nanoparticles due to the rapid growth in the number of parameters required to describe their 3D shape. Furthermore, the simulation parameters (population size, mutation density, ...) are difficult to standardise as they may differ significantly for each optimisation problem and genetic algorithm implementation. To this end, we have optimised the algorithm for computational efficiency and proposed simulation parameters which balance the need for mutations with the convergence rate such that the algorithm can reconstruct nanoparticles of up to at least 10 nanometres in size.
Results
Though the computational cost and choice of parameters of genetic algorithms, in general, is a whole area of study by itself, we have explored the behaviour for the specific application of reconstructing

the three-dimensional shape of nanoparticles. By choosing appropriate simulation parameters by balancing the mutation rate with the population size, we examine the scaling relationship of the convergence rate as a function of atomic columns in the image. A statistical analysis gives strong indications of a linear and well-behaved convergence rate.
Additionally, we used the algorithm to reconstruct a large simulated nanoparticle of approximately 10 nanometres in three dimensions with a high surface atom recovery. This demonstrates the capacity to reconstruct large nanoparticles with high accuracy and allows us to study the presence of specific surface features in such particles.

Conclusions

We have optimised and studied the performance of the Bayesian genetic algorithm for the reconstruction of nanoparticles at atomic scale with high accuracy. By doing so, we can reconstruct nanoparticles of up to at least 10 nanometres in size.

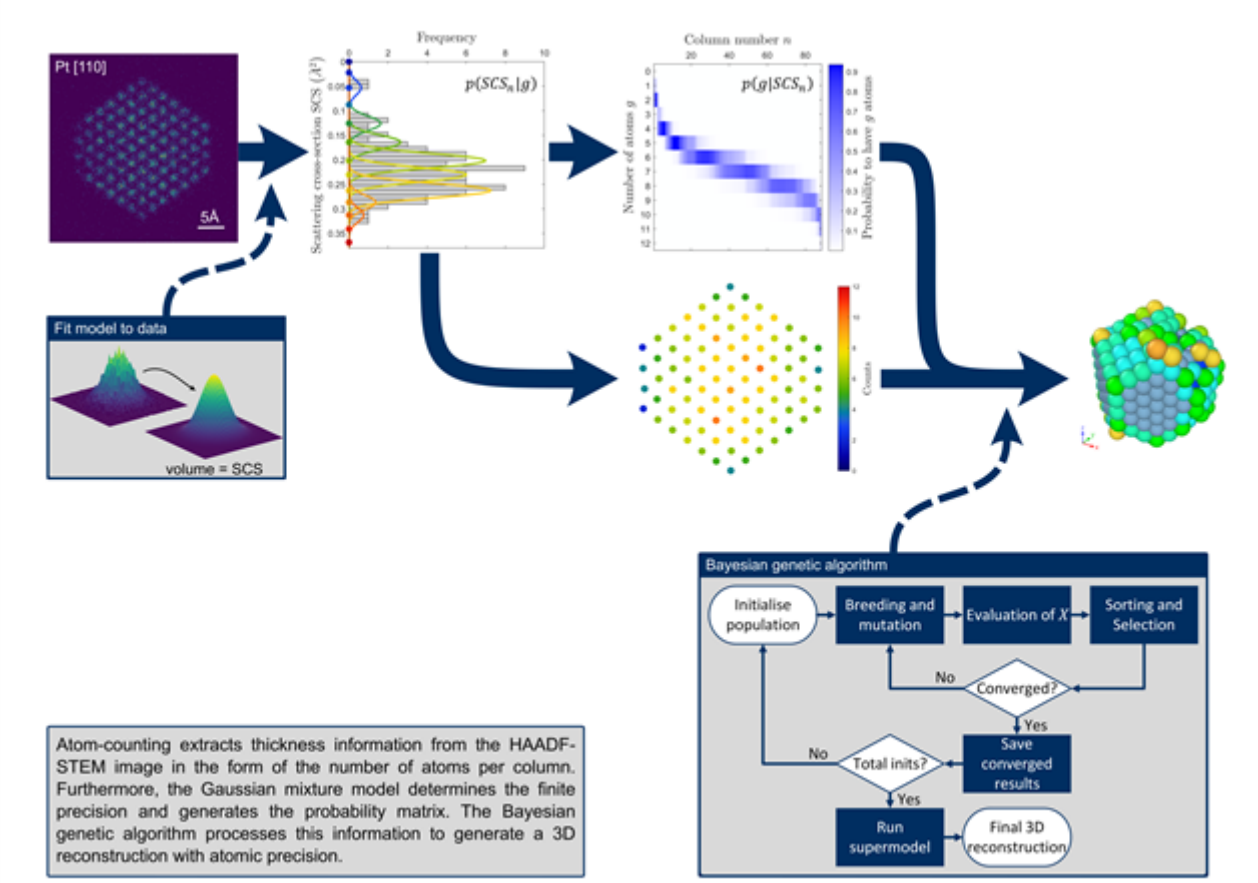

Keywords:

Quantitative HAADF-STEM, atom-counting, genetic optimisation

Reference:

S. Van Aert et al, Nature 470 374-377 (2011).
K. L. Mills et al, Evol Comput 23 309-342 (2015).
A. De Backer et al, Ultramicroscopy 171 104-116 (2016).
A. De Backer et al, npj Comput Mater 8 1–8 (2022).
A. De Backer et al, Ultramicroscopy 247 113702 (2023).

128

Unraveling the True 3D Structure of Colloidal Assemblies by Liquid Cell Electron Tomography

Daniel Arenas Esteban[1], Dr. Da Wang[1,2], Dr. Ajinkya Kadu[1,3], Mr. Noa Olluyn[1], Dr. Ana Sanchez Iglesias[4,5,6], Dr. Alejandro Gomez-Perez[7], Dr. Jesús Gonzalez Casablanca[8], Dr. Stavros Nicolopoulos[7], Prof. Luis M. Liz-Marzán[4,5,9,10], Prof. Sara Bals[1]
[1]Electron Microscopy for Materials Science (EMAT) and NANOlab Center of Excellence, University of Antwerp, Antwerp, Belgium, [2]Guangdong Provincial Key Laboratory of Optical Information Materials and Technology, South China Normal University, Guangzhou, China, [3]Centrum Wiskunde & Informatica (CWI), Amsterdam, The Netherlands, [4]CIC biomaGUNE, Donostia-San Sebastián, Spain, [5]Centro de Investigación Biomédica en Red, Bioingeniería, Biomateriales y Nanomedicina, CIBER-BBN, Donostia-San Sebastián, Spain, [6]Centro de Física de Materiales CSIC-UPV/EHU, Donostia-San Sebastián, Spain, [7]NanoMEGAS SRPL, Brussels, Belgium, [8]Universidad Rey Juan Carlos, Centro de Apoyo Tecnológico, Madrid, Spain, [9]Ikerbasque, Basque Foundation for Science, Bilbao, Spain, [10]Cinbio, Universidade de Vigo, Vigo, Spain

Poster Group 1

The colloidal bottom-up approach of nanoparticles self-assembling into ordered structures with tailored properties has recently attracted significant interest in various scientific fields. Therefore, their comprehensive structural and morphological characterization is essential, as the properties of these nanostructures are strongly correlated with their three-dimensional (3D) arrangement. Electron tomography is a common technique used for such nanoparticle characterization [1,2]. However, external forces that can affect the structure, such as the capillary forces caused by the common vacuum environment inside the microscope, are often neglected, resulting in misconnections between the obtained structure and the properties of the assemblies. As these materials are intended to be used in dispersion, our goal is to analyze the 3D arrangement of the assemblies in their native liquid environment. This innovative approach will allow us to establish a connection between the structure and properties of the assemblies under real working conditions.

In this contribution, we compare 3D reconstructions obtained in dry and liquid environments. We focus on two types of self-assemblies: gold NPs encapsulated in a polymeric shell and CTAB-coated gold nanorod bilayers. A commercial K-kit (Bio MA-TEK) liquid cell and a modified version with an increased angular tilt range (Tomochip [3]) were used depending on the assembly size. For larger assemblies, as the encapsulated gold NPs it is necessary to use larger window gap cells. However, this results in a larger background signal and limited tilt angles. On the other hand, smaller assemblies, such as the nanorods bilayers studied in this work, that can fit into the Tomochips, can benefit from a larger tilt range and lower background signal due to their reduced window gap.

The challenges of liquid-phase electron tomography have been addressed. Firstly, we adapted a fast acquisition approach to minimize the time and, therefore, the beam exposure of the sample, reducing possible beam damage. Secondly, we performed an interative denoise and rigid registration methodology to overcome challenges including increased background signal, low signal-to-noise ratios (SNR) resulting from scattering effects, and lengthy acquisition times required for two-dimensional (2D) projection images. Finally, we incorporate a compressed shape sensing method during 3D reconstruction to mitigate missing wedge artifacts from the limited tilt range and improve the SNR in the tilt series [4].

A comparison between similar 3D investigations performed in the native liquid environment and in dry state revealed a general decrease in interparticle distances in the latter. This effect can be

assigned to the compression effect of the capillary forces generated by the vacuum environment of the electron microscope during dry characterization. These observations emphasize the importance of conducting measurements under liquid-state conditions to accurately characterize NP self-assemblies and provide essential insights into the underlying physical and chemical mechanisms that govern these structures.

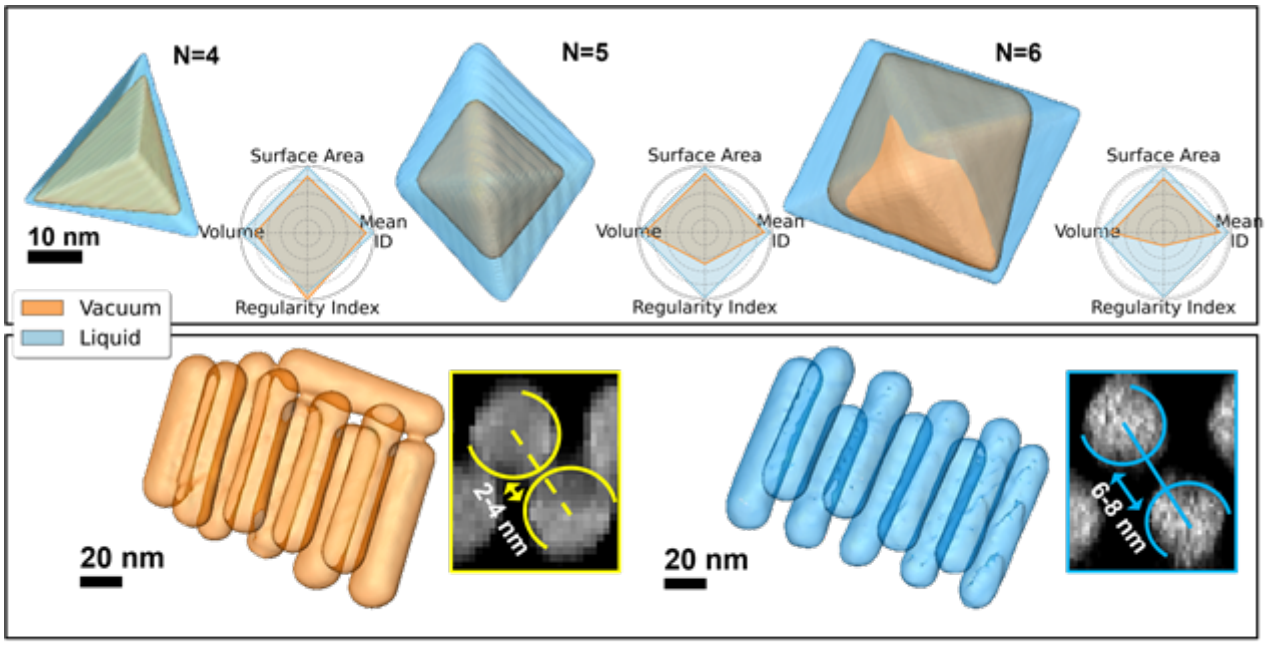

Figure 1. (top) Quantification analysis of the polyhedron formed by N=4, 5, and 6 on the gold NPs assemblies characterized in dry (orange) and liquid (blue) environments. (bottom) Interparticle measurements performed on the nanorod bilayers in dry (orange) and liquid (blue) environments.

Keywords:

Colloidal assembly, Tomography, Liquid TEM

Reference:

[1] D. Wang et al. Nat. Phys. 17 (2021), 128-134.
[2] T Altantzis et al. J. Phys. Chem. C 125 47 (2021) 26240-26246.
[3] P Das et al. Microscopy and Microanalysis 28 S1 (2022), 854-856.
[4] K. J. Batenburg et al. IEEE Transactions on Image Processing 20.9 (2011), 2542-2553.

184

Multi-scale characterization of vitamin B2 (riboflavin) supplements using X-ray Microscopy, SEM, and automated phase analyses

Ria Mitchell[1], Dr Darragh Murnane[2], Mr Andy Holwell[1]
[1]Carl Zeiss Microscopy Ltd, Cambourne, UK, [2]University of Hertfordshire, Hatfield, UK

Poster Group 1

Background incl. aims
Riboflavin is a water-soluble micronutrient that is essential for the reproduction of cells and growth in the human body, as well as helping to prevent inflammation and ageing. It naturally occurs in a variety of foods including fruit, vegetables and meats, however it is regularly incorporated into vitamin or dietary supplements to bolster healthy lifestyles. Recently, it has been found to potentially be a natural alleviator of migraines due to its preventative effects of migraine symptoms such as neuroinflammation, and now many migraine-relief specific versions of the nutrient exist and can be purchased 'off the shelf'. However, while most pharmaceutical products are highly regulated, dietary supplements such as these have less stringent regulatory assurances. The most popular cost-effective method of their production is from fermentation, where the active nutrient is subsequently mixed with other components such as anti-caking agents, fillers, and lubricants to homogenize the mix and ensure enough of the vitamin enters the body. However, different manufacturers include differing components in variable quantities, and there is variation in their manufacture. Therefore, a full multi-scale characterization of these supplements is important to (i) understand the spatial distribution and morphological characteristics of the different components, (ii) to quantify the active components, and (iii) to understand quality assurance based on the variable manufacturing processes involved with production of these supplements.

Methods
Here, we have studied two different vitamin B2 supplement capsules from two different manufacturers to characterize and quantify the different components in 3D. Capsule 1 contains riboflavin (active ingredient), silicon dioxide (likely as anti-caking agent), and Mg stearate (likely as lubricant), and capsule 2 contains riboflavin (active ingredient) and Mg stearate (likely as lubricant) only. We use X-ray Microscopy (XRM) to image the powders non-destructively in 3D, and apply various advanced reconstruction approaches to enhance visualization of the data: DeepRecon Pro, a machine-learning based reconstruction approach to reduce noise, improve contrast, and shorten scan time/increase throughput; and PhaseEvolve, which uses AI algorithms to enhance the data so that it uncovers different material contrasts uniquely revealed by XRM. Finally we use an automated phase classification and segmentation method to quantify the different components in 3D. This approach not only introduces the benefits of using 3D imaging to study pharmaceuticals, but sheds light on the structural morphology of the active components in vitamin supplements. Additionally, we use SEM in a correlative workflow for 2D imaging and chemical analyses of individual components.

Results
Both capsules' powders were imaged in 3D at the multi-scale using a ZEISS Xradia Versa 520 XRM. Initial observations reveal that the morphology of each capsules' powders are indeed very different, with large morphological and structural differences, suggesting that the powders were likely produced by two different production methods: spray drying and granulation. DeepRecon Pro significantly improves the quality of the data compared with tradiaitional reconstruction methods (e.g., filtered back projection) by reducing noise and improving contrast. PhaseEvolve further enhances the contrast between the different powder components, and we are able to identify an

additional ‘binder’ phase which is not identifiable from filtered back projection data alone, therefore contributing towards a more accurate segmentation of phases and data. Complementary analyses via Mineralogic 3D for phase classification indicates that this new binder phase is Mg stearate which is the ‘glue’ holding riboflavin particles together as agglomerates, and allows us to segment and quantify this phase fully in 3D. Further, using Mineralogic 3D we identify a filler (calcium phosphate) in capsule 1 which is not listed on the ingredients.

Conclusion

The results presented here show that non-destructive 3D imaging via X-ray Microscopy (XRM) and associated advanced reconstruction techniques are a useful tool for understanding the composition of vitamin supplements. We find previously unobservbable phases using these techniques, and are able to identify and quantify components which are not listed on the ingredients. This approach could be extended to other pharmaceutical materials to maintain regulation.

Keywords:

Pharmaceuticals, Tomography, materials characterization, AI

426

Quantification of chirality from electron tomography data

Robin Girod[1], Dr. Mikhail Mychinko[1], Kyle Van Gordon[2], Bing Ni[3,4], Francisco Bevilacqua[2], Luis Liz-Marzan[2,5,6,7], Sara Bals[1]
[1]EMAT and NANOlab Center of Excellence, University of Antwerp, Groenenborgerlaan 171, Antwerp B-2020, Belgium, , , [2]CIC biomaGUNE, Basque Research and Technology Alliance (BRTA), 20014 Donostia-San Sebastián, Spain, , , [3]Physical Chemistry, University of Konstanz, Universitätsstrasse 10, 78457 Konstanz, Germany, , , [4]Present adress: Department of Chemical Engineering, University of Michigan, Ann Arbor, MI USA, , , [5]Centro de Investigación Biomédica en Red, Bioingeniería, Biomateriales y Nanomedicina (CIBER-BBN), 20014 Donostia-San Sebastián, Spain, , , [6]Ikerbasque, Basque Foundation for Science, 48009 Bilbao, Spain, , , [7]CINBIO, University of Vigo, 36310 Vigo, Spain, ,

Poster Group 1

Background and aims.
Some optical nanomaterials exhibit the intriguing property of absorbing differently left- and right-handed polarized light. This optical handedness often arises from morphological chirality, the fact that mirrored shapes do not superimpose, but the quantitative relationships between morphology and optical properties are poorly understood. Establishing this knowledge requires accurate characterization the nanomaterials' morphology, as well as the calculation of chirality descriptors relevant to the optical properties of interest [1]. A prime example of such combination is the quantification of helicity from electron tomography (ET) three-dimensional (3D) reconstructions, which we previously presented [2]. Applied to wrinkled or twisted geometries such as those of chiral Au nanorods (NRs), this method informs about the helical character of the NRs and their handedness and is an excellent predictor of the sign of their circular dichroism (CD) spectra. However, helicity is a radially averaged measure, which limits its local interpretation, and entails strong geometrical assumptions, which limits its value for non-helical shapes even as they may still be chiral and exhibit clear optical handedness.
Here, we explored how different descriptors of chirality obtained from ET reconstructions can complement each other to link nanoscale morphology and optical handedness. To understand how local chiral features were varying, we first implemented a measure of their orientation, providing insights into both global and local handedness [3]. To overcome geometrical assumption, we then studied methods quantifying asymmetry on the basis of the difference between a geometry and its mirror image, including the Hausdorff chirality measure [1,4]. We finally tested if, beyond individual metrics, chiroptical performance could be statistically linked with a learned combination of morphological and chirality descriptors.
Methods.
As a prerequisite to study and establish chiral descriptors, a large dataset of ET reconstructions of chiral Au NRs was assembled. The particles in this dataset were typically 50-150 nm-long and were synthesized by seed-mediated growth. Two synthesis pathways were included: micelle-templating, whereby chiral micelles coil around achiral Au NR seeds, resulting in the growth of wrinkled particles whose helical morphology is characterized by a narrow pitch and a small helical orientation; chemical-inducing whereby chiral molecules such as amino-acids induce the preferential growth of high order, chiral surface facets. This latter approach yields highly helical, twisted structures with long pitches and high helical orientations when starting from single-crystalline seeds, but also strongly deformed, asymmetrical structures without clear geometrical handedness nor helical character but a handed optical signal when starting from pentatwinned seeds. In addition, the dataset includes the optical properties of all batches from which the particles are sampled, including absorption and CD spectra.

ET tilt-series were obtained in high angle annular dark field (HAADF) scanning transmission electron microscopy (STEM) and typically span 130-140° in 2 or 3° increments. 3D reconstructions were performed using the SIRT, expected maximization (EM) or constrained SIRT algorithms with in-house code or the ASTRA toolbox.
Surface orientation was computed using the ImageJ plugin OrientationJ while other computations and the statistical analyses were performed in python or Matlab with in-house code.
Results.
We first investigated how to obtain local analysis of the orientation of chiral features. Typically, chirality measures provide summary data, with a single metric indicating the degree of chirality and/or the handedness. Here, the orientation of chiral features on Au NRs was tracked and analyzed with spatial accuracy around the NR, evidencing local variations that were not visible when analyzing helicity (Figure, a-d).
To further quantify the chirality of non-helical structures, we investigated methods based on the calculation of the difference between a reconstruction and its mirror image. Such a descriptor effectively quantifies asymmetry, without considerations of handedness, and the difference is typically evaluated on the basis the Hausdorff distance, yielding the Hausdorff chirality measure. We found that optimizing for the minimum Hausdorff distance as required to calculate the measure requires long computation times if the full surface is used, limiting the applicability to simple shapes. As an alternative, we used a shape overlap measure (Figure, e-g), which can be calculated at a fraction of the cost. This method provided results similar to the Hausdorff chirality measure for classifying particles on the basis of their asymmetry and demonstrated that the morphology of non-helical structures could still be highly chiral (Figure, g-h), thus complementing helicity and orientation-based analyses.
Although powerful because of their simple interpretation, orientation, helicity and chiral distances are descriptors that provide part of the information only. We finally investigated if a combination, rather than a single descriptor, can predict optical properties from morphological data. Given the vast amount of data accumulated by our lab in the recent years, we will present how such combination could be learned statistically from ET reconstructions and the corresponding optical spectra.
Conclusion.
Beyond helicity, orientation tracking and asymmetry quantification provide insights into different aspects of morphological chirality. The key towards fully characterizing chirality might be in their adequate combination. Focusing on interpretable descriptors, this work expands the toolbox for microscopists to quantify chirality from ET reconstructions and paves the way towards establishing quantitative relationships between the morphology of chiral nanomaterials and their optical properties.

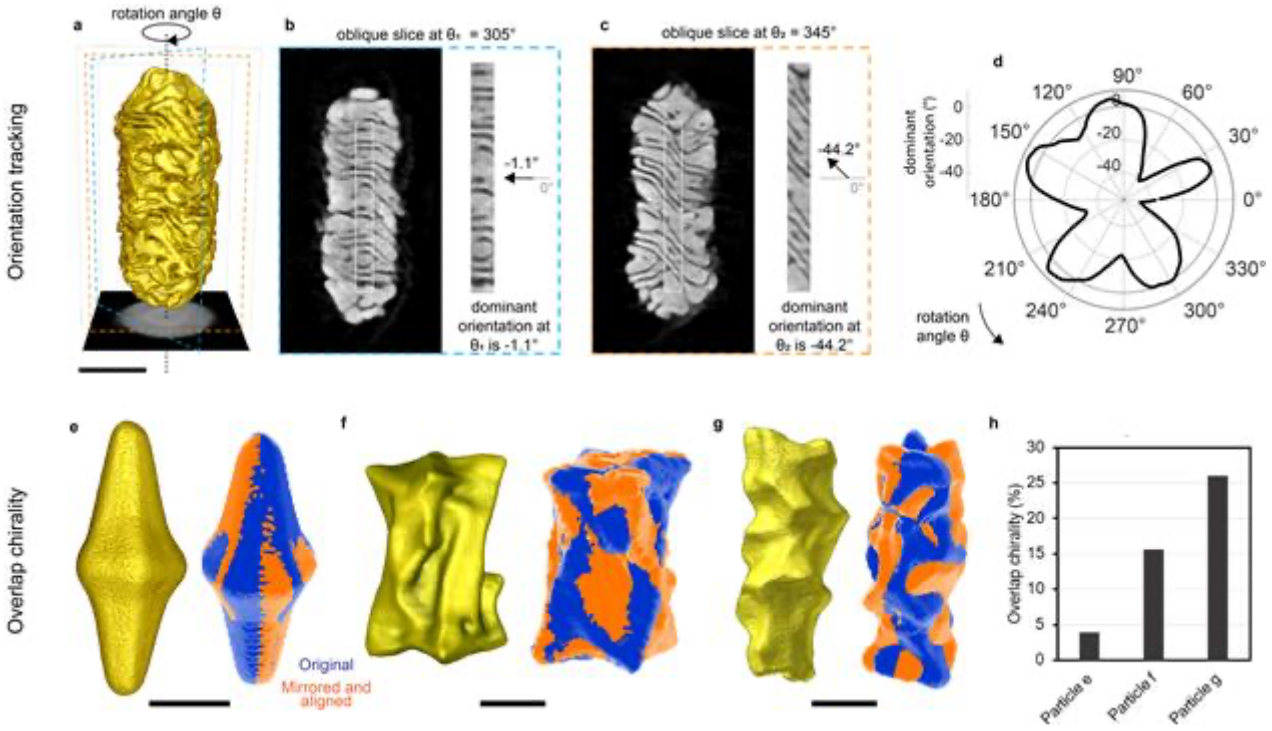

Keywords:

ET, tomography, plasmonics, chirality, descriptors

Reference:

1. Kim, J.-Y. et al. Assembly of Gold Nanoparticles into Chiral Superstructures Driven by Circularly Polarized Light. J. Am. Chem. Soc. 141, 11739–11744 (2019).
2. Heyvaert, W. et al. Quantification of the Helical Morphology of Chiral Gold Nanorods. ACS Materials Lett. 4, 642–649 (2022).
3. Van Gordon, K. et al. Single Crystal and Pentatwinned Gold Nanorods Result in Chiral Nanocrystals with Reverse Handedness. Submitted.
4. Buda, A. B. & Mislow, K. A Hausdorff chirality measure. J. Am. Chem. Soc. 114, 6006–6012 (1992)

588

Image fusion for 3D reconstruction of SEM images

Dr Turkka Salminen[1], Dr Lucio Azzari[1]
[1]Tampere Microscopy Center, Tampere University, Tampere, Finland

Poster Group 1

Background
Image fusion is commonly used in photography and optical microscopy to merge a stack of images taken with different focal lengths to produce a single in-focus image. It is necessary in applications where details of a single image are required to be as sharp as possible (e.g., medical imaging and surveillance), and where acquisition conditions are limited (e.g., when the scene depth is much larger than the system's focal length). There are several approaches and algorithms to determine the in-focus regions in each image of the stack. The algorithms can be grouped into three main categories: spatial domain, transform domain, and neural network [Bhat2021]. Furthermore, when the focus depth of each image is known, a depth map of the scene can also be estimated as a byproduct of the fusion algorithm. This depth map will contain information about the apparent distance of each object in the image.
Scanning electron microscopes are known for their improved depth of field over light microscopes and perhaps that is the reason why image fusion has seen little use with scanning electron microscopy images [Ersoy2008, Marturi2013]. However, the focal depth in SEM is known with high precision and the depth of field can be adjusted with the operating parameters of the microscope.
Methods
The focus of our work is twofold: 1) create an in-focus image using multiple SEM images acquired with different focal lengths and 2) use that information to estimate a depth value for each pixel of the resulting in-focus image. To do that, spatial domain image fusion algorithms are the most suitable for the task, because each output pixel is selected from one of the corresponding input pixels, and thus its focus depth is unequivocally determined by the focus depth of the image from which the pixel is chosen. Transform domain algorithms do not offer this possibility because the output image is usually a weighted sum of the input images in a particular transform domain. Furthermore, because the algorithm must be accessible, fast, and independent from the input data, we have decided not to use a neural network-based algorithm.
Our approach is based on the algorithm proposed by Haghighat et al., where the in-focus image is built by finding, pixel by pixel, which input image has the maximum local variance. This algorithm assumes that local variance and sharpness are directly correlated.
Our method can be divided into three mains steps:
1. Compute the magnitude of each input image gradient, that will then be used to estimate each input image local sharpness.
2. Run a sliding window of size 8x8 across all the gradient images; for each block we compute its variance, and we find and store in a 2D array the index of the input image with the largest local sharpness (i.e. largest local variance).
3. Smooth the array of indices with a low pass filter to make the output more consistent.
Results
The output from the above algorithm is a map that contains, for each output pixel, the index of the sharpest input image. From this index map we can construct the output in-focus image and its associated depth map (from focus).
Because we process the image block-wise, some blocky artifacts might occur at the borders of objects. To mitigate this problem, we propose an additional post-processing filtering of the depth map using the guided filter proposed by Sun et al. This filter aims at refining the depth map using the in-focus image as a pilot (like a bi-lateral filter).

The in-focus image and its depth map can finally be used to create a 3D point cloud of the imaged sample for the user to inspect it in three dimensions.

Conclusion

Our results indicate that this is a promising technique for visualization of SEM data and offers the possibility to determine the surface profile of samples. We will present our protocol for obtaining the image stacks, the procedure to create an in-focus image, depth map and a 3D point cloud from the data using the in-house built application.

Keywords:

SEM, Image fusion, 3D-reconstruction, Profilometry

Reference:

S. Bhat, D. Koundal, Multi-focus image fusion techniques: a survey, Artif Intell Rev 54, 5735–5787 (2021). https://doi.org/10.1007/s10462-021-09961-7

O. Ersoy, E. Aydar, A. Gourgaud, H. Bayhan, Quantitative analysis on volcanic ash surfaces: Application of extended depth-of-field (focus) algorithm for light and scanning electron microscopy and 3D reconstruction, Micron, 39, 128-136 (2008) https://doi.org/10.1016/j.micron.2006.11.010

N. Marturi, S. Dembélé and N. Piat, Depth and Shape estimation from focus in scanning electron microscope for micromanipulation, 2013 International Conference on Control, Automation, Robotics and Embedded Systems (CARE), Jabalpur, India, 1-6 (2013) https://doi:/10.1109/CARE.2013.6733694

M. B. A. Haghighat, A. Aghagolzadeh, H. Seyedarabi, Multi-focus image fusion for visual sensor networks in DCT domain, Computers & Electrical Engineering, 37, 789-797 (2011) https://doi.org/10.1016/j.compeleceng.2011.04.016

K. H. J. Sun, X. Tang, Guided Image Filtering, in IEEE Transactions on Pattern Analysis and Machine Intelligence, 35, 1397-1409 (2013) https://doi.org/10.1109/TPAMI.2012.213

596

Real-time undersampling optimization during electron tomography of beam-sensitive samples using golden ratio scanning and RECAST3D

Mr. Timothy Craig[1], Dr. Ajinkya Kadu[1], Prof. Dr. Kees Batenburg[2], Prof. Dr. Sara Bals[1]
[1]Electron Microscopy for Materials Science and NANOlab Center of Excellence University of Antwerp, Antwerp, Belgium, [2]Leiden Institute of Advanced Computer Science, Leiden University, Leiden, The Netherlands

Poster Group 1

Background
In recent years, nanomaterials have seen widespread usage in fields as diverse as biomedicines, energy storage and catalysis due to their unique chemical and physical properties. Hence, in-depth 3D characterization of these properties is critical to improving our understanding of nanomaterials and allows researchers to design nanomaterials better suited towards application. Electron tomography allows researchers to characterize the 3D volume of nanomaterials by acquiring a series of 2D projections at various angles (tilt series).1 Unfortunately, the acquisition of multiple projections to acquire a single 3D volume necessitates long acquisition times and electron beam exposure which can damage sensitive samples. To minimize such damage, researchers often try acquire fewer projections through tilt undersampling schemes, which can induce additional imaging artefacts. Therefore, it is important to determine the optimal number of projections that minimizes both beam exposure and undersampling artifacts for accurate reconstructions of beam-sensitive samples. Current methods for determining this optimal number of projections involve acquiring and post-processing multiple reconstructions with different numbers of projections, which can be time-consuming and requires multiple samples due to sample damage.2 Herein, we propose a novel workflow3 that combines a continuous acquisition scheme known as golden ratio scanning (GRS)4 with a quasi-3D real-time electron tomography software (RECAST3D)5 to simplify the process of tilt undersampling optimization.

Methods
To determine the optimum number of projections, a tilt series is collected continuously using GRS and a quasi-3D reconstruction is performed in real-time with RECAST3D. The reconstruction quality is determined using two metrics: i.) the signal to noise ratio and ii.) the change in the reconstruction as new projections are added. When the optimum reconstruction quality is achieved the acquisition is terminated. To validate this approach, the resulting optimum reconstruction is compared to a standard tomographic procedure for both a simulated structure undergoing beam damage and a Au nanoparticle. Finally, the application of this technique is highlighted by applying the technique to two beam sensitive metal-organic framework complexes: Au@NU-1000 and Au/Pd@ZIF-8.

Results
In both the simulated and experimental cases, the use of this methodology resulted in a significant improvement in reconstruction quality when compared to standard tomographic acquisition and comparable results to conventionally optimized tomography. However, whilst typical tilt-undersampling optimizing takes several acquisitions and post processing to perform, this workflow can achieve similar results during a single acquisition saving significant time for the microscopist.

Conclusions
Herein, we present a novel workflow for optimizing tilt undersampling during a single acquisition using GRS and real-time quasi-3D reconstruction. Simulated and experimental studies demonstrate that reconstructions of beam-sensitive samples optimized using this workflow have higher fidelity

with the pre-damaged sample than reconstructions using standard incremental acquisition. Through application to MOFs, we demonstrate that this approach can be used to effectively optimize imaging conditions of beam sensitive samples during a single acquisition.

Figure 1. Golden ratio scanning is used to acquire new projections which can be continuously added to the tilt series increasing sampling density. The reconstruction quality is monitored using a quasi-3D reconstruction software (RECAST3D) which quickly reconstructs 3 orthoslices during the acquisition. The acquisition can be arbitrarily terminated when the optimum reconstruction is obtained.

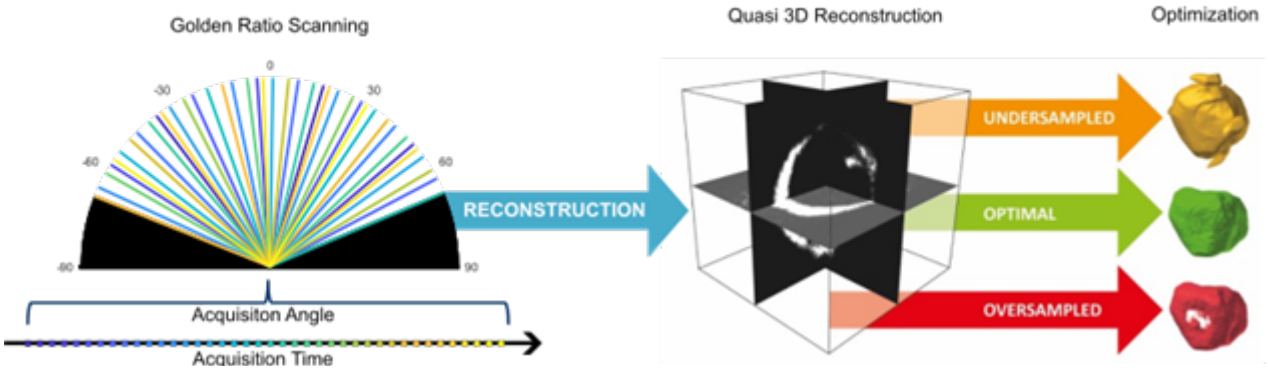

Keywords:

Electron Tomography, Beam Damage, MOFs

Reference:

(1) Weyland, M. Electron Tomography of Catalysts. Top. Catal. 2002, 21 (4), 175–183.
(2) Vanrompay, H.; Béché, A.; Verbeeck, J.; Bals, S. Experimental Evaluation of Undersampling Schemes for Electron Tomography of Nanoparticles. Part. Part. Syst. Charact. 2019, 36 (7), 1–8. https://doi.org/10.1002/ppsc.201900096.
(3) Craig, T. M.; Kadu, A. A.; Batenburg, K. J.; Bals, S. Real-Time Tilt Undersampling Optimization during Electron Tomography of Beam Sensitive Samples Using Golden Ratio Scanning and RECAST3D. Nanoscale 2023, 15 (11), 5391–5402. https://doi.org/10.1039/D2NR07198C.
(4) Münch, B. Spatiotemporal Computed Tomography of Dynamic Processes. Opt. Eng. 2011, 50 (12), 123201. https://doi.org/10.1117/1.3660298.
(5) Vanrompay, H.; Buurlage, J. W.; Pelt, D. M.; Kumar, V.; Zhuo, X.; Liz-Marzán, L. M.; Bals, S.; Batenburg, K. J. Real-Time Reconstruction of Arbitrary Slices for Quantitative and In Situ 3D Characterization of Nanoparticles. Part. Part. Syst. Charact. 2020, 37 (7). https://doi.org/10.1002/ppsc.202000073.

629

Deep image prior for limited-angle electron tomography

Dr Zineb SAGHI[1], Laure Guetaz[2], Thomas David[2], Philippe Ciuciu[3], Zineb Saghi[1]
[1]Univ. Grenoble Alpes, CEA, Leti, F-38000, Grenoble, France, [2]Univ. Grenoble Alpes, CEA, Liten, F-38000, Grenoble, France, [3]Univ. Paris Saclay, CEA-NeuroSpin, INRIA, Parietal, Gif-sur-Yvette, France

Poster Group 1

Background incl. aims

Electron Tomography (ET) is a widely used technique for the 3D characterization of nanomaterials. To obtain faithful reconstructions, high-quality projection data must be acquired over the full 180° tilt range and at tilt increments of 1-2°. However, for slab-like sample geometries, the tilt range is often limited due to geometric restrictions within the TEM, and a large tilt increment is used to minimize the total electron dose. These restrictions lead to blurring and distortions in reconstructions obtained with conventional algorithms such as simultaneous iterative reconstruction technique (SIRT). Compressed sensing (CS) approaches have been introduced to improve the quality of reconstructions. Although CS techniques outperform conventional methods in sparse-view acquisition scenarios, they fail to correct artifacts due to the limited angular range. Data-driven deep learning (DL) approaches have been proposed for denoising and distortion correction of X-ray tomography and ET reconstructions. Although promising, these approaches are highly dependent on the availability of high-quality data sets for neural network training. Such data sets are often not available in practice, making it difficult to apply DL methods to a wide range of samples. Recently, Deep Image Prior (DIP) has been proposed for several image restoration problems, and adapted to limited-angle X-ray tomography. The method uses a neural network as a prior for the reconstruction, but has the advantage of not requiring any training data set, making it suitable for ET applications.

Methods

In this work, we apply DIP with total variation regularization (DIP-TV) to a sample consisting of carbon-supported platinum nanoparticles (NPs) dispersed on a carbon grid. ADF-STEM and HAADF-STEM tilt series were acquired from -60° to +60° with an increment of 2°, using an FEI Titan Themis operating at 200kV. In HAADF-STEM projections, only Pt NPs were visible, while in ADF-STEM mode, both Pt NPs and C support were visible but the images were affected by diffraction contrast. DIP-TV was applied for 3D reconstruction in both imaging modes, using increments of 2°, 10° and 20°. Results were compared with those obtained with SIRT and CS with TV regularization (CS-TV).

Results

Figure 1 shows the reconstruction of a slice from ADF-STEM and HAADF-STEM tilt series, obtained with SIRT, CS-TV and DIP-TV. The tilt range is [-60°:+60°] for all reconstructions, with the missing wedge in the horizontal direction, while the tilt increment is set to 2°, 10° and 20°. In HAADF-STEM reconstructions (left), only Pt NPs are visible. SIRT suffers from elongation artifacts and ‘star artifacts’ as the tilt increment increases. CS-TV slightly improves the quality of the reconstructions but suffers from oil painting effects. DIP-TV reconstructions appear consistent under all acquisition conditions, with near-spherical, well-contrasted particles. The ADF projections are more complex, as the carbon support is visible and superposed on the Pt NPs. SIRT reconstructions suffer from significant artifacts in the support, which increase as the number of projections is reduced. CS-TV still manages to reconstruct the particles, but the carbon is not well retrieved. In particular, for both SIRT and CS-TV reconstructions, the carbon appears heterogeneous and porous below and above each NP. This is probably due to the non-linear intensity in ADF images (diffraction contrast). In contrast, DIP-TV retrieves near-spherical NPs and a homogeneous carbon support, under all acquisition conditions. Using 20° increment (7 projections in total), the shape of the carbon is slightly distorted on the right-hand side, but the technique largely outperfoms SIRT and CS-TV.

Conclusion

This work shows the robustness of DIP-TV for ET using a limited number of projections and a restricted tilt range. The method benefits from the power of neural network architecture, but requires no training data set, making it suitable for ET and extremely versatile since it can be used under different acquisition conditions. Moreover, the method could be applied to different modalities of the same material and potentially directly for 3D reconstruction.

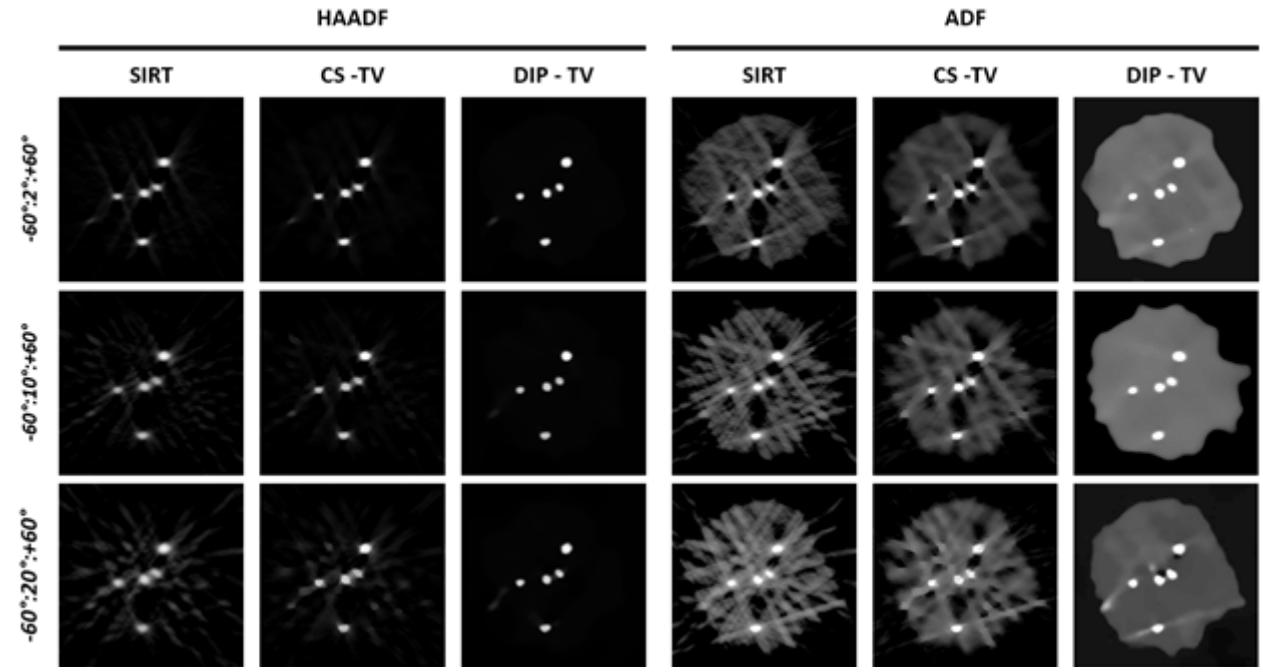

Keywords:

Electron Tomography, Reconstruction, Deep Learning

Reference:

M. Jacob et al., Ultramicroscopy 2021, 225:113289.
Y. Jiang et al., Ultramicroscopy 2018, 186:94.
D. Ulyanov et al., International journal of computer vision 2020, 128 :1867.
D. Baguer, et al., Inverse Problems 2020, 36.9 :094004.
This work, carried out on the Platform for Nanocharacterisation (PFNC), was supported by the “Recherche Technologique de Base” and "France 2030 - ANR-22-PEEL-0014" programs of the French National Research Agency (ANR).

708

Improving electron tomography of mesoporous silica structures by Ga intrusion

Thomas Przybilla[1], Johannes Böhmer[1], Alexander Kichigin[1], Moritz Buwen[1], Alexander Götz[1], Dominik Drobek[1], Jakob Söllner[2], Matthias Thommes[2], Benjamin Apeleo Zubiri[1], Erdmann Spiecker[1]
[1]Institute of Micro- and Nanostructure Research (IMN) & Center for Nanoanalysis and Electron Microscopy (CENEM), Department of Materials Science and Engineering, Friedrich-Alexander-Universität Erlangen-Nürnberg, Erlangen, Germany, [2]Institute of Separation Science and Technology, Department of Chemical and Biological Engineering, Friedrich-Alexander-Universität Erlangen-Nürnberg, Erlangen, Germany

Poster Group 1

Background incl. aims:
Mesoporous silica structures are widely used in the field of nanotechnology, e.g. as substrate in heterogeneous catalysis [1] and as stationary phase material in size-exclusion chromatography [2]. To understand and improve the material's properties, a precise characterization of the pore network is indispensable. Common approaches to quantitatively analyse the mesoporous space are averaging sorption/intrusion techniques [3] and three-dimensional imaging techniques such as electron tomography in high-angle annular dark-field (HAADF) scanning transmission electron microscopy (STEM) mode [4]. While the first mentioned techniques lack the localized spatial information, HAADF-STEM tomography resolves the mesoporous structure with a spatial resolution in the nm-range, but suffers from poor contrast between pore space and network in case of low atomic number (Z) materials, since the imaging contrast scales with ~Z^2 [1]. In this study, we uniquely combine Ga intrusion of the pore space in mesoporous silica with HAADF-STEM tomography to enhance the Z-contrast between pores and silica significantly by a factor of ~9x. This enables a reliable quantitative analysis and visualizes localized information about the pore network and the process of Ga intrusion. In particular, we apply 360° HAADF-STEM tomography on pillar-shaped specimen prepared from the intruded mesoporous silica. This allows for precise 3D reconstruction of the tilt series without missing-wedge artifacts to accurately obtain important pore characteristics such as size distribution, tortuosity, and connectivity [5].

Methods:
Mesoporous silica with an average pore size of 20nm is intruded with Ga up to different filling degrees (50%, 100%) by a modified Hg intrusion porosimetry technique. From the intruded sample systems pillar-shaped specimen are prepared on a tip by scanning electron microscopy (SEM)/focused ion beam (FIB) techniques using a Helios NanoLab 660 DualBeam SEM-FIB. The samples are analysed by 360° HAADF-STEM tomography in a double Cs-corrected FEI Titan³ Themis at 300 kV.

Results:
Backscattered electron (BSE) imaging on a FIB prepared cross-section of the fully intruded silica reveals that the method of Ga intrusion leads to a homogeneous filling of the pore space in a representative volume required for STEM tomography (Figure 1a - left). The homogeneous distribution of the infiltrated Ga phase is crucial for a reliable quantitative analysis by STEM tomography. If the pressure during the intrusion process is reduced, a partial filling (50%) of the porous network can be achieved with the empty pockets being evenly distributed in the entire sample (Figure 1a - right). This finding resembles the homogenous and narrow pore size distribution of the material and hints towards smaller pore channels being present within the unfilled spaces, since the infiltration of smaller pore channels requires in general higher pressures.

From the fully- and half-intruded silica, pillar-shaped specimen can be prepared on tomography tips by common FIB lift-out technique (Figure 1b). In contrast, imaging and pillar preparation from pure silica is challenging, since the material is electron-beam sensitive and non-conductive. This leads to sample charging and causes sample drift and uneven milling during FIB preparation. Therefore, a charge neutralizer is indispensable in case of silica, which is, however, not available on any FIB instrument. Also during STEM tomography, charging effects occurring on pure silica easily cause complications resulting in bending and structure deformation, which strongly worsen the 3D reconstruction quality. Moreover, the build-up of carbon contamination during tilt series acquisition worsens the image contrast over time, due to the low atomic number difference of Si, O, empty space and C contamination in HAADF-STEM imaging mode. In contrast, specimen intruded with Ga feature a ~9x stronger contrast, so that C contamination is negligible and the pore and silica space can clearly be resolved throughout the entire tilt series (Figure 1c). As outlined, Ga intrusion of mesoporous silica features multiple advantages: (1) it improves the imaging contrast in HAADF-STEM mode, (2) increases the sample integrity, (3) mechanically stabilizes the pillar, and (4) forms a conductive pathway through the sample eliminating charging effects during preparation and STEM tomography. These benefits improve significantly the reconstruction quality of the tomographic tilt series in the fully intruded specimen (Figure 1d - left), facilitate the phase segmentation between Ga and silica (Figure 1d - middle) and enable a reliable quantitative analysis of the porosity and pore size distribution by the method of maximum sphere inscription (MSI) (Figure 1d - right, Figure 1e). For a benchmark comparison, the mesopores of the silica structures were investigated with N_2 physisorption, evaluated with the non-local density functional theory (NLDFT) method. Moreover, we investigated the 3D reconstruction of the half-intruded silica specimen (Figure 1f) to improve our knowledge regarding the Ga intrusion process and to study contrast differences of pores, Ga and silica in more detail. While the filled channels are clearly visible, the unfilled channels, which indicate bottlenecks in the pore pathways, are weakly distinguishable from the surrounding silica network (Figure 1f - left). The respective segmentation is challenging, but helps to identify bottlenecks in the pore pathways (Figure 1f - right). In sum, the findings from electron tomography can further elucidate the gallium intrusion process on the nanoscale and contribute to the development of methods for textural characterization based on liquid intrusion.

Conclusion:
This study highlights the potential of Ga intrusion for contrast enhancement of the pore space in mesoporous silica during 360° HAADF-STEM tomography to study quantitatively important pore characteristics. Vice versa, the study further helps to understand the process of Ga intrusion. The intrusion process leads to a homogeneous Ga distribution and enhances the mechanical stability of the non-conductive silica during both FIB sample preparation and acquisition of the STEM tilt series by minimizing electrical charging. The Ga intrusion process can be regarded as a potential common technique to improve electron tomography not just on mesoporous silica but also on various other porous materials.

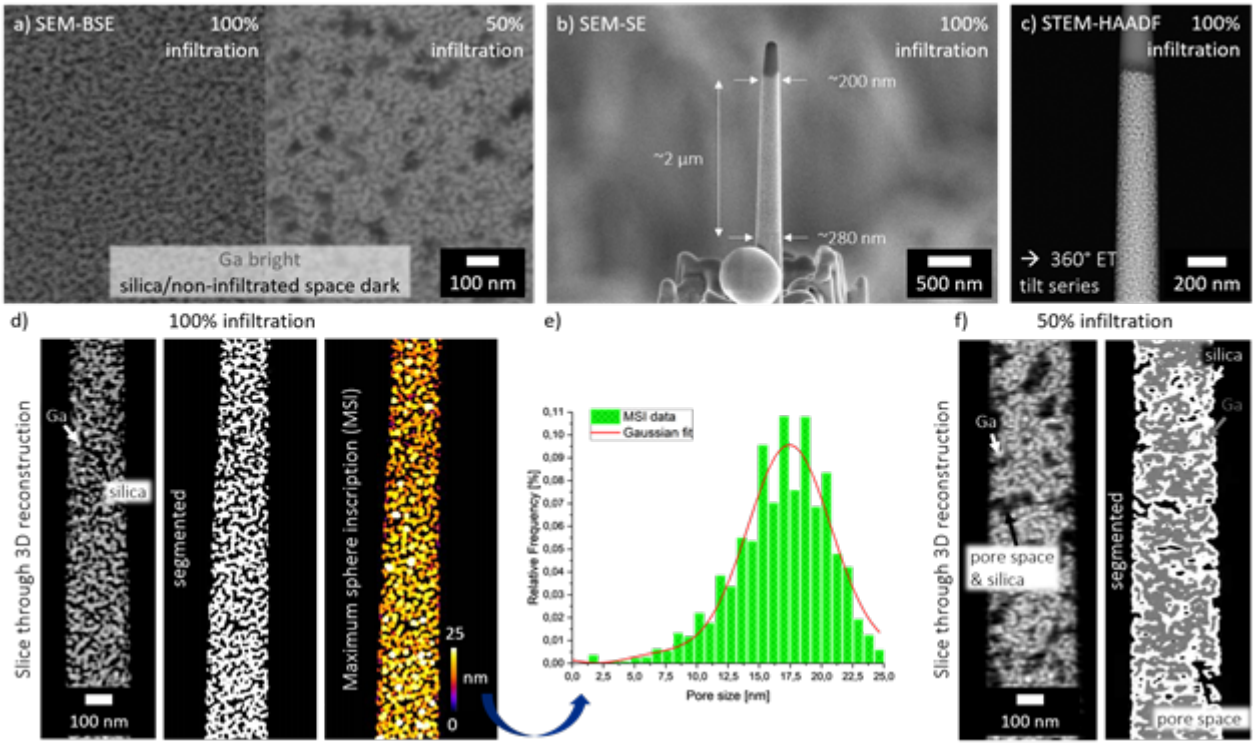

Keywords:

360° ET, quantitative pore analysis

Reference:

[1] D. Ozkaya, W. Zhou, J. M. Thomas, P. Midgley, V. J. Keast, and S. Hermans, Catalysis Letters 60 (1999), 113-120.
[2] Y. Zhao, J. Wang, Y. Yang, Q. Fu, Y. Ke, Journal of Chromatography. A 1664 (2022), 462757.
[3] C. Schlumberger, C. C. Collados, J. Söllner, C. Huber, D. Wisser, H.-F. Liu, C.-K. Chang, S. A. Schuster, M. R. Schure, M. Hartmann, J. I. Siepmann, M. Thommes, ACS Applied Nano Materials 7 (2024), 1572-1585.
[4] B. ApeleoZubiri, J. Wirth, D. Drobek, S. Englisch, T. Przybilla, T. Weissenberger, W. Schwieger, E. Spiecker, Adv. Mater. Interfaces 8 (2021), 2001154.
[5] X. Huang, D. Hlushkou, D. Wang, U. Tallarek, C. Kübel, Ultramicroscopy 243 (2023), 113639.

715

Momentum-resolved STEM Tomography of Gold-Silver core-shell Nanoparticles

Sebastian Sturm[1], Dr. Felizitas Kirner[2], Prof. Dr. Elena Sturm[2], Prof. Dr. Knut Müller-Caspary[1]
[1]Ludwig-Maximilians-Universität München, Department of Chemistry, Munich, Germany, [2]Ludwig-Maximilians-Universität München, Department of Earth and Environmental Sciences, Munich, Germany

Poster Group 1

Background

Precisely tailored Gold-Silver core-shell (Ag@Au) Nanoparticles (NPs) can have outstanding optical properties due to localized surface plasmon resonances, making them suitable candidates for advanced senors or for application in photothermal therapy [1]. Exact control over the nanocrystal growth however, demands for suitable analytic methods to confirm the quality and reproducibility of the synthesis. Facetted core-shell NPs like this especially benefit from techniques like Electron Tomography and STEM Tomography in particular, which are able to reconstruct their nanoscopic structures in all three dimensions, via acquisition of a tilt series of projections [2].
Depending on the detectors used, STEM offers a great variety of suitable signals for these projections [3]. For example the commonly used Bright-field (BF), annular dark-field (ADF) and high-angle annular dark-field (HAADF) signals each cover rings with different radii, corresponding to certain magnitudes in momentum space. However, the exact radii of the detector in momentum space additionally vary with the chosen camera length and the choice of those radii in the experiment has significant impact on the fidelity of the tomographic reconstruction, since most techniques rely on the linearity of the signal during projection and might even have different optima for detecting different materials. To understand the impact of the detector choice and to overcome its limitations, Momentum-resolved STEM (MR-STEM or 4D-STEM) has been applied, where for each scan position of a 2D scan raster an individual 2D diffraction pattern is recorded with the help of a fast direct electron detector and signals for each magnitude of momentum have been extracted from this data set. This allows to apply and compare arbitrary virtual detectors post-experimentally. In combination this enables MR-STEM Tomography, where the best suitable signal with respect to its performance in tomographic reconstruction of the Ag@Au NPs can be determined in hindsight.

Methods

The MR STEM experiments were conducted using a probe corrected FEI Titan Themis operated at 300kV and equipped with a Quantum Detectors MerlinEM direct electron detector (based on Medipix 3).
Acquisition of the 4D tilt series has been done using an in-house developed software written in python, utilizing the FEI Scripting COM interface. A 4D tilt series with a tilt range of -75° .. +72.5° in 2.5° steps has been recorded with 256 x 256 scan points and 256 x 256 pixel diffraction patterns at an semi-convergence angle of 18mrad. For reconstruction, a WSIRT reconstruction algorithm has been used with 5 to 10 iterations.

Results

The performance of different detector radii in momentum space in regards of tomographic reconstruction has been investigated on reconstructions of selected slices. Additionally an magnitude of momentum resolved WSIRT reconstruction of the whole volume has been explored, leading to a 4D dataset (x, y, z,|k|), which can then be evaluated e.g. using Principal component analysis (PCA). Furthermore the second moment in momentum space has been calculated, where ring segments with radius k have been weighted with k^2, summing up from a chosen minimum radius to a cut-of

radius. Figure 1 exemplary shows the reconstructed Second Moment tomogram (c) of four self-assembled Ag@Au NPs (b), clearly depicting the octahedrally faceted Au cores encapsulated by truncated cubically faceted Ag shells.

Conclusion

Momentum-resolved STEM has been explored to find the most suitable signal for STEM Tomography, comparing different ADF / HAADF signals. For the Ag@Au NPs, the second moment has proven to quickly converge to similar results as the HAADF signal reconstructions, if the outer detector radius is chosen large enough, however the less strict dependence on the inner radius might still be advantageous for some applications.

Figure 1:
Momentum Resolved STEM Tomography of Gold-Silver Core-Shell Nanoparticles:
a) HAADF STEM overview image
b) HAADF STEM image of the region of interest, highlighted in (a)
c) Second moment tomogram as an example of momentum resolved STEM tomography.

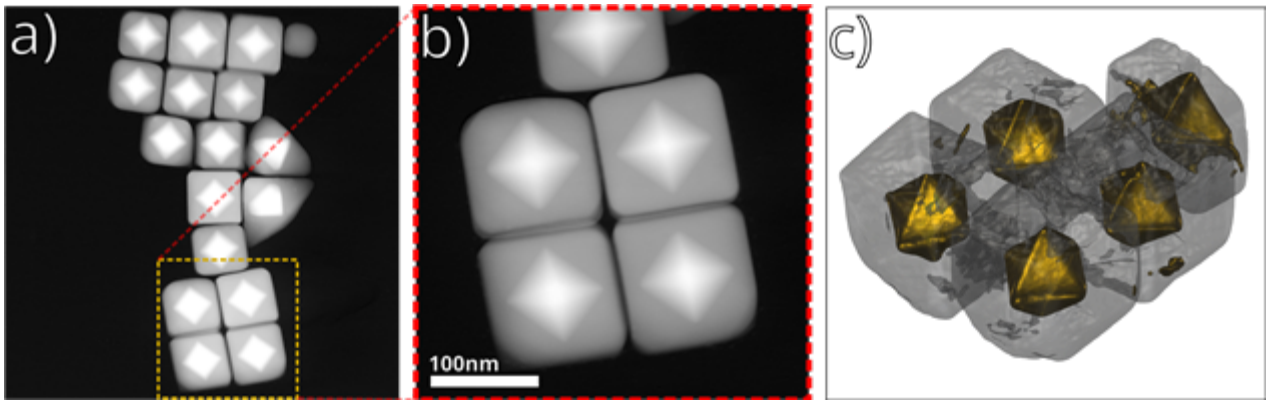

Keywords:

STEM Tomography, 4D STEM

Reference:

[1] J SCHULTZ, et al., Adv. Optical Mater. 2021
[2] M WEYLAND, et al. Materials Today, 2004,
[3] H ROBERT, et al. Ultramicroscopy, 2022,

743

Deep Learning assisted X-ray Microscopy Characterization of Nickel based Metal Matrix composite reinforced with TiC

Dr. Kaushik Yanamandra[1], Dr. Hrishikesh Bale[1], Dr. Rajarshi Banerjee[2], Ria Mitchell[1]
[1]Carl Zeiss Research Microscopy Solutions, Dublin, United States of America, [2]Materials Science and Engineering, University of North Texas, Denton, United States of America

Poster Group 1

Background
Metal Matrix Composite (MMC) are a class of materials with remarkable mechanical, thermal, and electrical properties. These composites consist of a metallic matrix reinforced with ceramic or other non-metallic phases. Reinforced MMC are of interest in many applications due to their multifunctionality, which yields combinations of properties such as high specific strength, stiffness and toughness, and a low coefficient of thermal expansion [1]. Ni-Ti-C based metal matrix composites explored in this paper is produced using the laser engineered net shaping (LENS) process presenting a unique hierarchical microstructure consisting of an in situ formed and homogeneously distributed titanium carbide (TiC) phase reinforcing the nickel matrix [2]. Additionally, by tailoring the Ti/C ratio in these composites, an additional graphitic phase can also be engineered into the microstructure. The resulting three-phase Ni-TiC-C composites were comprehensively characterized using Deep learning assisted X-ray Microscopy (XRM). By analyzing the microstructure at the sub-micron level, XRM enables the understanding of the spatial distribution and alignment of reinforcing phases within the metal matrix.
Method
Ni-Ti-C-based MMCs were fabricated using the laser engineered net shaping (LENS) process. The LENS process involves the deposition of metal powder layers using a laser beam, allowing precise control over the composition and microstructure. XRM, with its high-resolution and non-destructive capabilities, provides valuable insights into MMCs. Notably, certain phases within the titanium carbide (TiC) domains push the limits of X-ray microscopy detection, relying on X-ray-to-visible-light conversion via scintillators coupled with optical magnification objectives. To overcome previous limitations, a unique combination of specially designed high-resolution objectives and deep-learning-based 3D reconstruction was utilized. The combination of new generation scintillator technology and integrated deep-learning reconstruction known as DeepRecon [3] enable sub-micron resolutions in dense and large MMC sample.
Results
Ni-Ti-C based MMC exhibits intricate microstructures that span a wide range of length scales, with various phases playing a critical role in determining its exceptional properties. Leveraging the high-resolution and non-destructive capabilities of X-ray microscopy the microstructure of the MMC is studied and analyzed in 3D at different length scales. The X-ray microscopy images reveal the spatial arrangement of TiC phases within the metal matrix. Features of <.0.1µm were previously undetectable in large and dense samples due to their small size and due to the noise produced in a tomography scan from these samples were observed using the DeepRecon – Deep Learning based reconstruction algorithm. The findings from XRM data significantly enhance the understanding of MMCs.
Conclusion
These composites hold promise for various engineering applications, including aerospace, automotive, and structural components. The study of Ni-Ti-C-based MMCs not only provides insights into the relationship between microstructure and properties but also set forth a vital tool and technology needed to understand these intricate structures. X-ray microscopy emerges as a powerful tool for MMC analysis, offering high resolution and non-destructive capabilities. Its application

enhances the comprehension of MMC performance, thus opening new avenues for their optimized design and engineering.

Keywords:

Metal Matrix Composites, X-ray Microscopes

Reference:

1. Zheng, B., Topping, T., Smugeresky, J.E. et al. The Influence of Ni-Coated TiC on Laser-Deposited IN625 Metal Matrix Composites. Metall Mater Trans A 41, 568–573 (2010). https://doi.org/10.1007/s11661-009-0126-5
2. Borkar, Tushar, et al. "Laser-deposited in situ TiC-reinforced nickel matrix composites: 3D microstructure and tribological properties." Jom 66 (2014): 935-942.
3. Andrew, Matthew, et al. "Fully automated deep-learning-based resolution recovery." 7th International Conference on Image Formation in X-Ray Computed Tomography. Vol. 12304. SPIE, 2022.

843

Advanced acquisition strategies for lab-based diffraction contrast tomography

Florian Bachmann[1], Jun Sun[1], Jette Oddershede[1], Erik Lauridsen[1]
[1]Xnovo Technology ApS, Køge, Denmark

Poster Group 1

Background incl. aims
Non-destructive imaging of a polycrystalline material's 3D grain microstructure is key to a better understanding of the material performance and to validating computational models for predicting the material behavior. In addition, an integrated microstructural modeling approach, ensuring the handshake between modeling and experimentation, relies on adequate experimental statistics of 3D sample volumes that are representative in both size and shape.

Methods
In this study, we exploit lab-based diffraction contrast tomography (DCT) [1,2] to experimentally map the 3D grain structure. The introduction of three new advanced acquisition strategies for lab-based DCT – named Helical Phyllotaxis, Helical Phyllotaxis Raster, and Helical Phyllotaxis HART – enables grain mapping of longer, larger, as well as high-aspect ratio samples [3]. The implementation of these advanced acquisition strategies combines a golden angle rotation with vertical and horizontal translations to perform a seamless data collection that has a uniform sample illumination both angularly and spatially. Reconstruction of the corresponding data is equally seamless, simultaneously using all data to reconstruct the full illuminated volume without the need for stitching of data subsets or sample subvolumes.

Results
We will present and discuss different acquisition strategies with emphasis on how to approach a given acquisition problem inherent to the sample. Particular emphasis will be on the Helical Phyllotaxis HART (high-aspect ratio tomography for plate-like samples) strategy that enables investigations of a hitherto inaccessible class of sample geometries comprising industrially relevant materials like rolled metal sheets and electrical steels [4].

Conclusion
The advanced acquisition strategies take lab-based non-destructive 3D grain mapping to the next level of throughput, grain statistics and versatility. While the throughput warrants 4D studies of materials microstructural evolution, a representative sample volume is a prerequisite for successful model predictions, and the versatility enables studies of samples or components under more realistic in situ or in operando conditions.

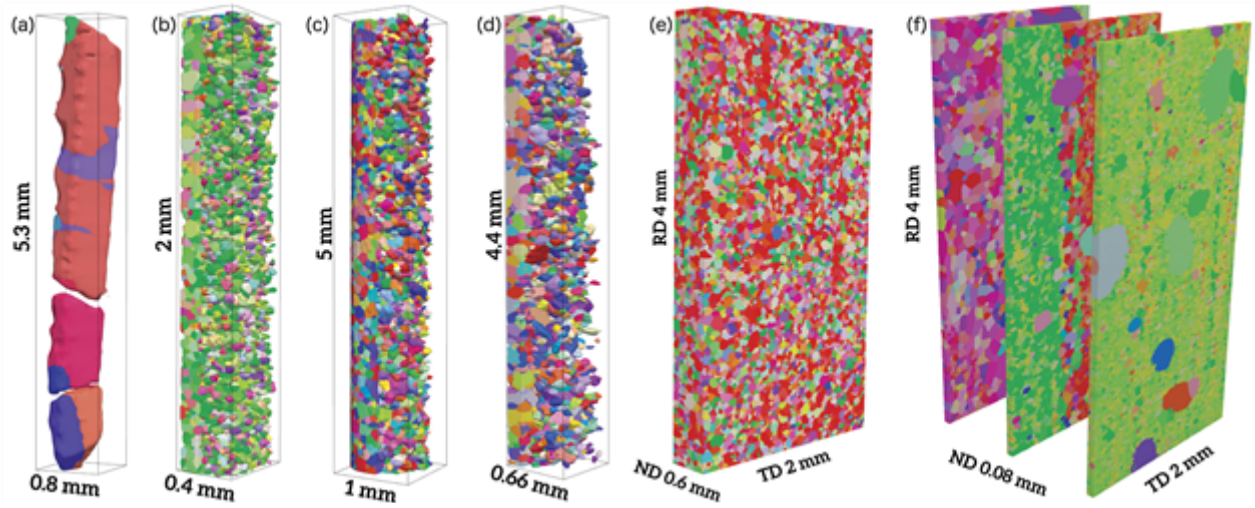

Keywords:

Lab-based DCT, Advanced Acquisition

Reference:

[1] Holzner, C., et al., doi: 10.1017/S1551929516000584 (2016).
[2] Bachmann, F., et al., doi: 10.1107/S1600576719005442 (2019).
[3] Oddershede, J., et al., doi: 10.1007/s40192-021-00249-w (2022).
[4] Sun, J., et al., doi: 0.1007/s40192-021-00245-0 (2021).

860

4D-STEM Optical Sectioning of Dopants in Diamond

Mr. Aidan Horne[1], Mr. Jacob Lewis[1], Mr. Emmanuel Tegegne[1], Dr. Peng Wang[1]
[1]University of Warwick, Coventry, United Kingdom

Poster Group 1

Due to improvements of aberration correctors in scanning transmission electron microscopes (STEM), larger convergent semi-angles can be used as more of the probe can be collected without introducing aberrations to the image. These larger convergent semi-angles lead to two notable improvements in the reconstructed image; an improved lateral resolution and a reduced depth of field [1]. The benefits of a better lateral resolution are immediately obvious, but by reducing the depth of field, new methods of imaging can be obtained, namely optical sectioning [2]. Optical sectioning involves collecting many micrographs of a sample with varying defocus which allows for investigation into the third dimension of the material instead of the two lateral dimensions as in conventional STEM. Four dimensional scanning transmission electron microscopy (4D-STEM) builds on conventional STEM by using superfast pixelated detectors to collect the entire diffraction pattern which allows us to reconstruct the sample using different methods such as conventional reconstructions like high angle annular dark field (HAADF) as well as more advanced methods, only available to 4D-STEM such as centre-of-mass (COM) imaging and ptychography. Here we present a body simulation work to investigate the efficacy of optical sectioning through a range of 4D-STEM data reconstruction techniques and a range of dopants within the sample.
Simulations are done using the ab initio simulation software plugin abTEM which utilizes the multislice algorithm [3]. Using this software we generate 4D-STEM datasets with a 200kV accelerating voltage and a convergence angle of 30mrad. For this work, the probe aberrations are set to zero to match ideal imaging conditions. The samples used were diamond crystal of 15nm thickness with different substitutional and interstitial dopants of masses ranging from 14Si to 82Pb. The location in the z direction of these dopants was also varied to investigate efficacy of the techniques dependent on the depth of the dopant within the sample.
The reconstruction techniques used here consist of HAADF which has been the standard for imaging heavy elements within materials since the contrast of HAADF reconstructions follows a power law of z^n where 1≤n≤2 [4]. Common 4D-STEM techniques are also implemented. COM which works by finding the average deflection of the probe by the sample in the diffraction plane, as well as its subsidiaries, integrated centre of mass (iCOM) and differentiated centre of mass (dCOM). Furthermore, the recently proposed technique of symmetry STEM (S-STEM) which involves investigating the symmetry of the diffraction pattern by rotating or reflecting the diffraction pattern and cross correlating it with the original diffraction pattern to reconstruct [5].
Using the techniques described we find that different imaging methods excel depending on the relative weight of the dopant compared to the bulk crystal. As expected, HAADF provides a simple and effective method for imaging heavier atoms regardless of position in the crystal. The comparison is less clear when investigating lighter atoms such as silicon. In these regimes methods such as iCOM and dCOM prove themselves to be powerful tools for finding the location of the atom within the structure. We find that S-STEM is less of an effective tool than the others described, but this may be a poor representation of the true case, since relaxation of the crystal lattice may lead to strain in the sample for which S-STEM has been suggested to be a useful tool for identifying point defects [5]. It still may be an unreliable tool for optical sectioning though since S-STEM is robust at reconstructing atomic resolution images regardless of defocus as we have demonstrated with our results, as symmetry is independent of defocus.
The methods here result in a detailed analysis of how utilizing all the variables and tools available when imaging these materials using 4D-STEM can be leveraged to obtain the best results for optical

sectioning. This work focuses on diamond as a bulk crystal within which dopants are placed so could be used as an effective framework for investigating the composition of colour centres such as nitrogen and silicon vacancy centres.

Figure 1: (a), (b) and (c) shows COM, dCOM and iCOM reconstructions of diamond respectively with germanium dopant within box drawn on (a). (c) and (e) show line profiles of (b) and (c) along the line drawn. (f) Schematic of diamond view down <100> zone axis with Cu dopant place on the top surface, middle and bottom surface of the crystal, respectively. (g) S-STEM reconstruction of the lattice shown in (f) with 180o rotation of the diffraction pattern, red line shows path of line profile shown in (h). (h) Intensity line profile of S-STEM reconstruction with different dopants/vacancies in the crystal.

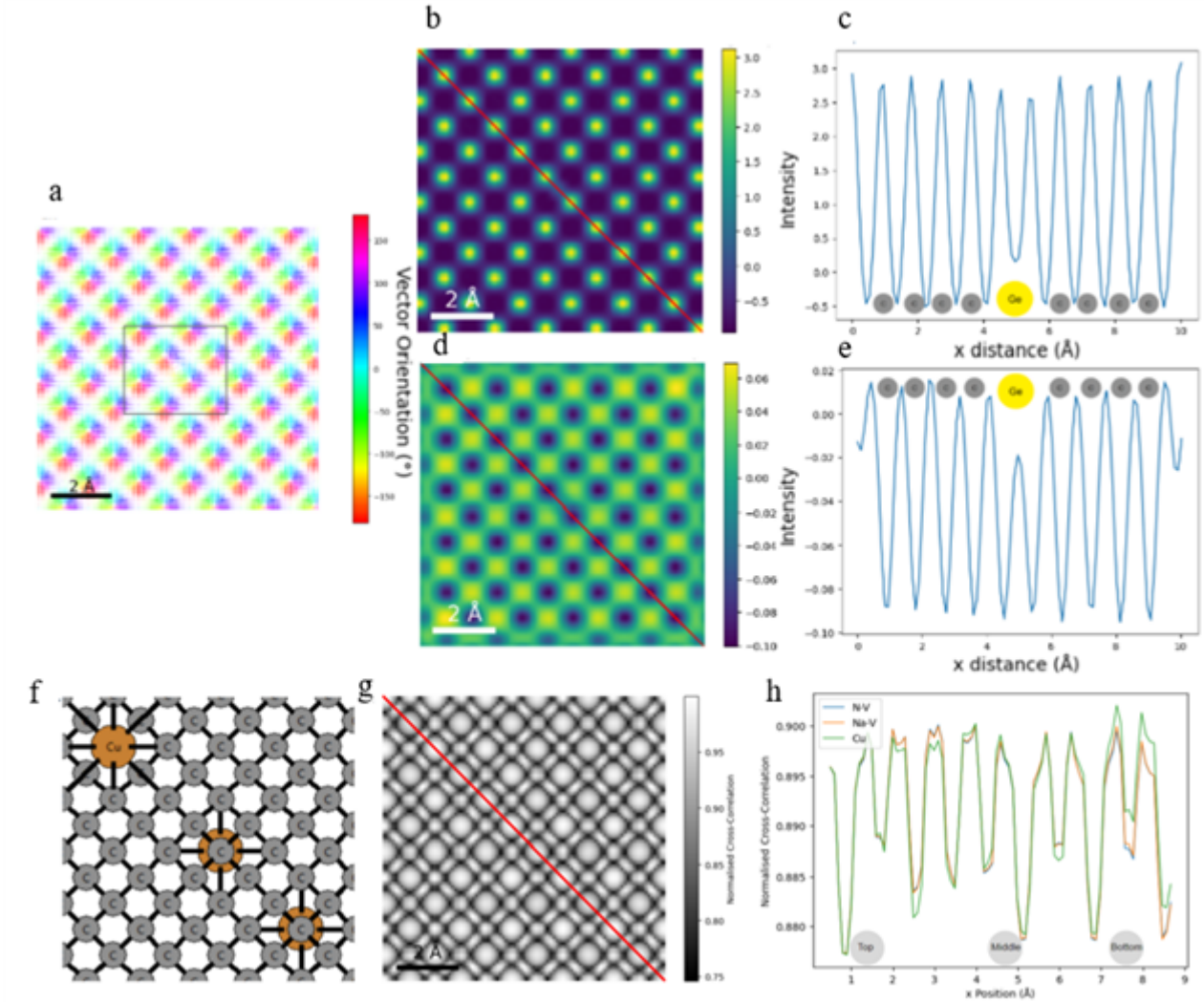

Keywords:

4D-STEM, iCOM-STEM, Optical Sectioning, 3D-Imaging

Reference:

[1] M. Born & E. Wolf, Elsevier, 2013.
[2] M Krajnak & J Etheridge, Proc. Natl. Avad. Sci. USA.2020;117(45) 27805-27810.
[3] J.Madsen & T. Susi, Open Research Europe 1:24 (2021).
[4] S. Bals et al. Ultramicroscopy, 104 (2005), 105.
[5] G. Behan et al. Phil. Trans. R. Soc. A. 367: 3825-3844.

878

Understanding field evaporation sequences by in-situ correlative microscopy and simulation

Mohammed Ilhami[1], Prof. Williams Lefebvre[1], Prof. Francois Vurpillot[1]
[1]Groupe De Physique Des Matériaux, Saint Etienne Du Rouvray, France

Poster Group 1

Background

Atom Probe Tomography (APT) provides detailed information on a material's microstructure and its chemical composition. This technique enables access to the 3D position and chemical nature of each atom in a sample. The process involves evaporating the atoms using an electric field and reconstructing a 3D model of a needle-shaped specimen. However, the resolution of APT can be degraded for heterogeneous materials by artifacts potentially associated with the reconstruction methods. Furthermore, the geometric model of the hemisphere on a truncated cone used for APT reconstructions relies on assumptions about variations in the tip curvature along the evaporation sequences. These fluctuations depend on variations in the evaporation field, which are governed by the distribution of areas of higher or lower evaporation field in the sample. This is for instance illustrated in Figure 1.
Tracking the shape of the APT tip during evaporation can provide valuable information about the tip radius, which can help improve the reconstruction algorithm, mapping the electric field around the tip can also indicate areas of higher or lower electric field. In-situ correlative electron microscopy, achieved by performing APT experiments in a STEM can consequently help understanding the evaporation sequences.

Methods

4D-STEM [1] experiments were carried out on a polarized Al-Fe APT tip subjected to 1 kV. A CheeTah Timepix3 pixelated detector was used to record a diffraction pattern for each pixel as the tip was scanned. To mitigate dynamic diffraction effects, a precession angle of 0.7 degrees was used.
Data analysis was performed using the Libertem [2] software. For simulating the field evaporation process, we utilized the Robin-Rolland [3] algorithm that calculates the electric charge on each atom and predicts evaporation events by identifying atoms that reach a critical evaporation field threshold.

Results

Our experiments showed variations in electrostatic fields around a polarized Al-Fe tip, subjected to a voltage of 1 kV. This variation is shown in Figure 2. The analysis shows a constant electrostatic field inside the tip, indicated by the blue color. A high field was observed near the apex of the tip, indicating a high probability of evaporation, confirmed by the results of simulation, represented in Figure 3.

Conclusion

In this study, we have developed an approach that makes it possible to follow the shape of an APT tip during evaporation, by performing APT experiments in a (S)TEM. In situ correlative microscopy was achieved by developing a sample holder capable of applying a voltage of up to 8 kV. In addition, 4D-STEM experiments made it possible to visualize the electrostatic field on a polarized APT tip. These results could help improve the accuracy and 3D reconstruction of atom probe data. The integration of numerical modeling can be used to predict material behavior during APT analysis and to confirm experimental results.

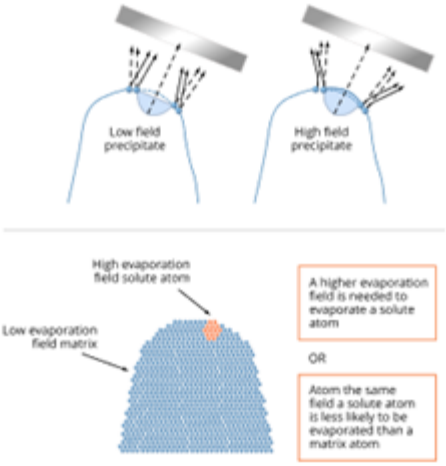

Figure 1: Illustration of effects of high and low field precipitate on the ion trajectories.

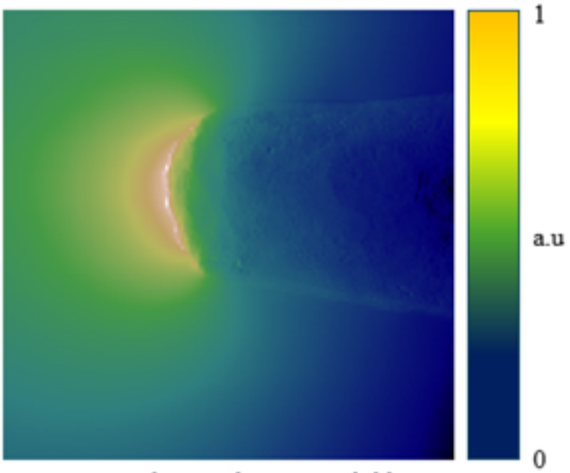

Figure 2: Qualitative electrostatic field map of a polarized Al-Fe sample, with an applied voltage of 1 kV.

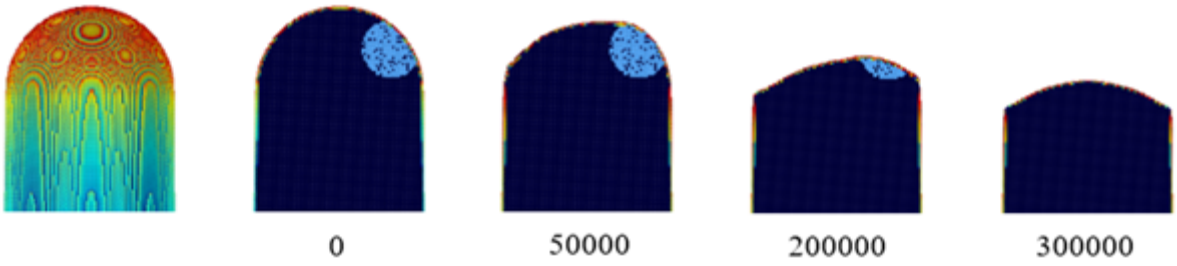

Figure 3: Evaporation sequences of a simulated Al-Fe tip with a high field precipitate.

Keywords:

APT, (S)TEM, In-situ correlative microscopy

Reference:

[1] C. Ophus, « Four-Dimensional Scanning Transmission Electron Microscopy (4D-STEM): From Scanning Nanodiffraction to Ptychography and Beyond », Microsc Microanal, vol. 25, no 3, p. 563-582, juin 2019, doi: 10.1017/S1431927619000497.

[2] A. Clausen et al., « LiberTEM: Software platform for scalable multidimensional data processing in transmission electron microscopy », JOSS, vol. 5, no 50, p. 2006, juin 2020, doi: 10.21105/joss.02006.

[3] B. Klaes et al., « A model to predict image formation in the three-dimensional field ion microscope », Computer Physics Communications, vol. 260, p. 107317, mars 2021, doi: 10.1016/j.cpc.2020.107317.

894

Simulating iDPC tomography of CeO2 nanoparticles with experimentally realistic parameters and conditions

Miss Ella Kitching[1], Dr Thomas Slater[1]
[1]Cardiff Catalysis Institute, School of Chemistry, Cardiff University, Cardiff, United Kingdom

Poster Group 1

Background incl. aims
Electron Tomography (ET) is a 3D analysis technique that produces a 3D reconstruction from a tilt series of microscopy images at 1-5° increments. Electron tomography can be used to characterise the 3D structure of nanoparticles at atomic resolution from an input of 40-150 images, depending on the specific reconstruction algorithm and parameters. Atomic electron tomography has been possible with HAADF-STEM for over a decade (Scott et al., 2012) . However, a limitation of the technique is that prolonged exposure to the electron beam can cause damage or changes to samples, prohibiting an accurate reconstruction.
Integrated Differential Phase Contrast (iDPC) imaging is a technique which has contrast proportional to atomic electrostatic potential captured using a segmented detector. iDPC provides a better signal-to-noise ratio than HAADF at similar electron doses due to use of the bright-field disk and allows for atomic-resolution imaging with lower electron doses. iDPC additionally enables simultaneous imaging of light and heavy atoms, due to its image contrast being proportional to Z rather than Z^2 as in HAADF (Lazić et al., 2016).
Atom and defect positions at the surface of nanoparticles are crucial to catalytic performance. Accurate characterisation of 3D structure can therefore explain trends in catalytic activity/selectivity and assist in the rational design of catalysts. iDPC provides an excellent technique to image light atoms and their vacancies, even alongside atoms of higher atomic number. This is particularly valuable in the imaging of metal oxides, where surface termination and surface defect density can greatly impact catalytic properties.
We aim to demonstrate that an iDPC atomic resolution ET reconstruction is able to provide the locations of oxygen atoms, in addition to metal atoms within a nanoparticle. To investigate this, we simulate tilt series of iDPC and HAADF images, and generate tomographic reconstructions of a CeO_2 nanoparticle. CeO_2 was chosen due to its prevalence in catalysis and its requirement of a flux lower than $7x10^5$ $e^-nm^{-2}s^{-1}$ to avoid beam damage (Johnston-Peck et al., 2016).
With these reconstructions, we assess the ability of iDPC tomography to distinguish between oxygen-terminated and cerium-terminated surfaces, and to detect surface oxygen vacancies. Additionally, we demonstrate that iDPC will produce accurate tomographic reconstructions when applied at lower doses, resulting in reduced beam damage, compared to HAADF tomography.
Method
Atomic models of octahedral ceria nanoparticles of lengths of 3 nm and 7 nm are built using the Python package Atomic Simulation Environment (ASE), using an additional Python package (Wulffpack) to adjust particle truncation based on surface energies.
iDPC-STEM and HAADF-STEM images of these models are simulated using the PRISM algorithm within the Python package abTEM (Madsen & Susi, 2020). We define set values of semiangle cutoff (17.5 mrad for iDPC, 30 mrad for HAADF), accelerating voltage (200 kV), PRISM interpolation factor (4) and collection angle (13-56 mrad for iDPC, 56-200 mrad for HAADF). A total of 151 images are simulated with tilt angles ranging from ±75°. The effects of finite electron dose (via Poisson noise) and partial spatial coherence (via Gaussian noise) are added in post-processing.
3D reconstruction is performed using the ASTRA toolbox, applying the ASTRA-SIRT algorithm. TVM and GENFIRE reconstruction algorithms are also compared when using reduced numbers of

projections. Reconstructions are formed with 1, 3 or 5° increments between each image. Determination of atom intensities in the resulting reconstructions are performed through ImageJ.

Results

Oxygen atoms were clearly distinguishable in the tomographic reconstructions of the iDPC images (without the addition of noise). The SIRT iDPC reconstruction had a Ce:O intensity ratio of 170:60 compared to 135:5 for HAADF. The iDPC reconstruction additionally displayed a 177.6% intensity increase when comparing the locations of surface oxygens to vacancies, enabling clear differentiation between oxygen atoms and vacancies. This visible difference is demonstrated in the attached reconstruction slice graphic.

Partial spatial coherence (source size 0.2 – 0.4 eV), and finite electron doses (50 – 50000 e^- /Å²) were applied to successfully demonstrate the impact of these conditions on the quality of tomographic reconstructions. This has been quantified by measuring atom intensities in the reconstruction and assessed qualitatively by comparing the ability to visually distinguish individual oxygen atoms and vacancies without further processing. We plan to additionally assess aberrations (such as defocus).

The SIRT iDPC reconstruction with a dose per image of 5000 e^- /Å² and a source size of 0.3 eV had a 256.50% intensity increase of the locations of surface oxygens compared to vacancies, showing vacancy detection is still feasible under low-dose experimental conditions. This reconstruction also displayed a Ce:O intensity ratio of 104:44, compared to 23:5 for a HAADF reconstruction under the same conditions. This HAADF reconstruction contained no visible oxygens, as expected.

These simulations confirm the resolution limits of different acquisition conditions for iDPC tomography, enabling experimental application of optimum conditions, and a known error margin to operate within.

Conclusions

Simulating iDPC and HAADF-STEM tomography has successfully confirmed parameters and requirements for atomic resolution iDPC tomography, enabling future experimental applications. By confirming the lower dose requirement for iDPC tomography, we have demonstrated the ability to create tomographic reconstructions of beam-sensitive samples which could not be captured with HAADF tomography.

We have additionally confirmed the ability of iDPC-STEM tomography to distinguish between vacancies and oxygen and cerium atoms within a 3D reconstruction of a CeO_2 nanoparticle. This demonstrates the potential of iDPC-STEM tomography as a technique for analysis of the surface termination of metal oxides, detection of oxygen vacancies and support-nanoparticle interface analysis.

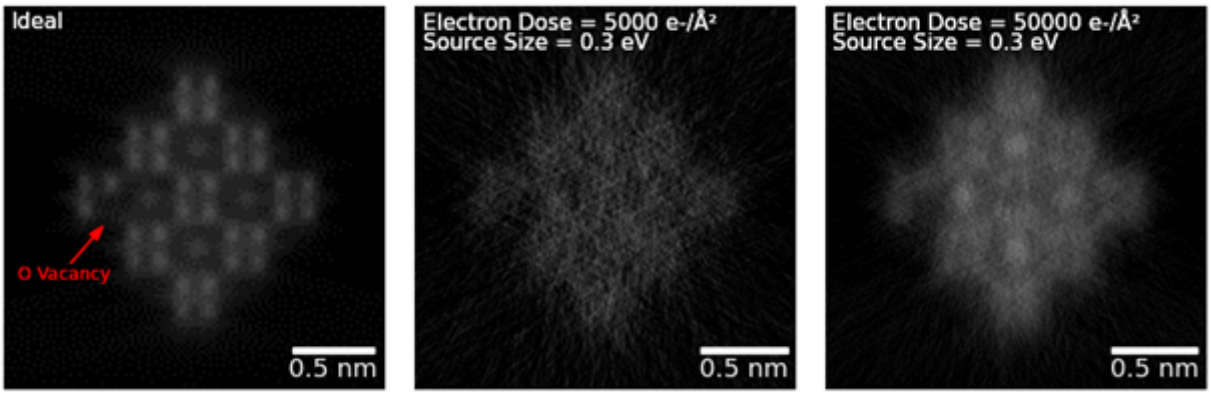

Keywords:

Tomography, Python, iDPC, Simulation, Low-dose

Reference:

Johnston-Peck, A. C., DuChene, J. S., Roberts, A. D., Wei, W. D., & Herzing, A. A. (2016). Dose-rate-dependent damage of cerium dioxide in the scanning transmission electron microscope. Ultramicroscopy, 170, 1–9. https://doi.org/10.1016/j.ultramic.2016.07.002
Lazić, I., Bosch, E. G. T., & Lazar, S. (2016). Phase contrast STEM for thin samples: Integrated differential phase contrast. Ultramicroscopy, 160, 265–280. https://doi.org/10.1016/j.ultramic.2015.10.011
Madsen, J., & Susi, T. (2020). abTEM: ab Initio Transmission Electron Microscopy Image Simulation. Microscopy and Microanalysis, 26(S2), 448–450. https://doi.org/10.1017/S1431927620014701
Scott, M. C., Chen, C.-C., Mecklenburg, M., Zhu, C., Xu, R., Ercius, P., Dahmen, U., Regan, B. C., & Miao, J. (2012). Electron tomography at 2.4-ångström resolution. Nature, 483(7390), 444–447. https://doi.org/10.1038/nature10934

903

Complementary vEM approaches for ultrastructural changes during the development of D. melanogaster germline intercellular bridges

Dr Irina Kolotuev[1], Abigayle Elsbury[2], Caroline Kizilyaprak[1], Stephanie Pellegrino[2], Dr Lindsay Lewellyn[2]
[1]Faculté de Biologie et de Médecine, Université de Lausanne, Lausanne, Switzerland, [2]Department of Biological Sciences, Butler University, Indianapolis, USA

Poster Group 1

Background and aims
The fruit fly Drosophila melanogaster is an excellent model for studying biological processes, and many questions in cell and developmental biology have been answered using this system. Incomplete cytokinesis is an essential process studied in many cell types which allows cells to form stable intercellular bridges that connect them to each other. Although intercellular bridges are found in somatic and germ cells throughout the animal kingdom, the most well-studied are those within the developing egg chamber. Many essential pathways and processes are required to allow the egg chamber to develop into a mature fly egg. The egg chamber consists of a cluster of 16 interconnected germ cells surrounded by a layer of somatic cells. Following each of the four germ cell divisions that create the germ cell cluster, the midbody is re-organized to form a stable intercellular bridge or ring canal. These ring canals undergo significant growth, which allows cytoplasmatic contents and nutrients to be transferred from supporting nurse cells to the growing oocyte. Although fluorescence and electron microscopy-based studies have been used to study the role of ring canal proteins during oogenesis, a complete ultrastructural characterization of these structures is lacking.
Methods
Electron Microscopy is a powerful tool for imaging cellular structures at the nanoscale, providing valuable insight into the ultrastructure of many cell and tissue types. Volume microscopy techniques such as Focused Ion Beam, Scanning Block Face, and Array Tomography have considerably advanced the potential applications of SEM-based approaches. To learn more about ultrastructural changes in the ring canals throughout oogenesis, we have used a combination of complementary vEM approaches – FIB-SEM to monitor the early stages of oogenesis and AT-SEM to follow the structures in later stages of oogenesis. We have aligned and segmented the stacks of images to analyze the structure of the ring canals during the development of the egg chamber.
Results
By using a complementary set of vEM-based approaches, we were able to visualize ultrastructural changes in the germline ring canals throughout oogenesis. We segmented the large data set collected using Focused Ion Beam SEM to generate a complete 3D model of the germarium and an early-stage egg chamber. The combination of AT-SEM and FIB-SEM allowed us to gain insight into previously unappreciated aspects of ring canal structure and function. In addition, we have characterized the microvilli meshwork surrounding the ring canal structures (Figure). These structures have been proposed to be essential to anchor the ring canals within the nurse cell membranes, but such a detailed three-dimensional view of their orientation has not been produced.
Conclusions
This combination of complementary vEM approaches allowed us to capitalize on the strengths and overcome the limitations of each individual approach. This modern framework could be used to answer biological questions in other tissues or organisms that face similar technical challenges; for example, in older egg chambers, the ring canals are very small structures within a large sample volume. Our work illustrates the potential scientific insight that can be provided by a high-content dataset, which could potentially become a valuable resource for further analysis by additional groups

in this field. Although the focus was on ultrastructural changes in the germline RCs, our dataset contains valuable details of additional cell types and structures.

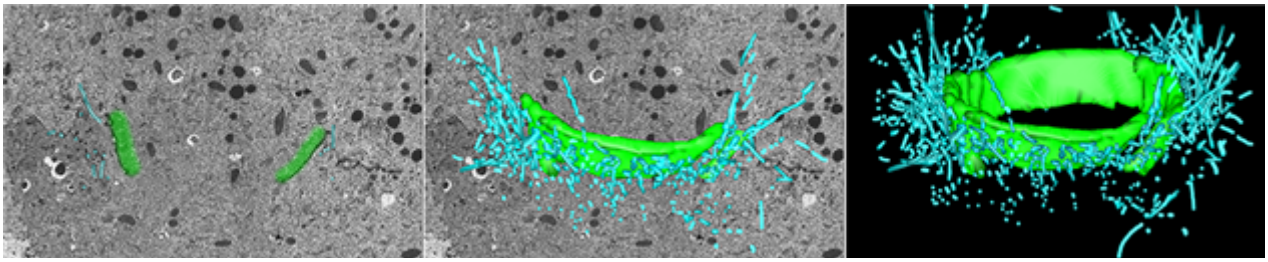

Keywords:

EM, 3d, ArrayTomo, segmentation, Drosophila

Reference:

Kolotuev I. Work smart, not hard: How array tomography can help increase the ultrastructure data output. J Microsc. 2023 Aug 25

Franke T, Kolotuev I. Array Tomography Workflow for the Targeted Acquisition of Volume Information using Scanning Electron Microscopy. J Vis Exp. 2021 Jul 15;(173)

Thestrup J, Tipold M, Kindred A, Stark K, Curry T, Lewellyn L. The Arp2/3 complex and the formin, Diaphanous, are both required to regulate the size of germline ring canals in the developing egg chamber. Dev Biol. 2020 May 1;461(1):75-85.

Kline A, Curry T, Lewellyn L. The Misshapen kinase regulates the size and stability of the germline ring canals in the Drosophila egg chamber. Dev Biol. 2018 Aug 15;440(2):99-112

1071

Investigation of GaAs-based nanowire heterostructures using tomography based on STEM-HAADF tilt-series[1]

Richard Zell[1], Sebastian Sturm[1], Hyowon W. Jeong[2], Prof. Gregor Koblmüller[2], Prof. Knut Müller-Caspary[1]
[1]Ludwig-Maximilians-Universität, Munich, Germany, [2]Technical University of Munich, Munich, Germany

Poster Group 1

In the development of on-chip electronics, group III/V semiconductor nanowires (NWs) hold great interest, due to their small footprint allowing compatibility with lattice mismatched substrates like silicon while greatly increasing the chemical flexibility.[2] Within this work GaAs-NWs with optically active axial InGaAs heterostructures and an AlGaAs capping layer are investigated. These spatially confined optical cavity structures facilitate low loss propagation of optical modes and show a high refractive index contrast.[3] We aim to create a better understanding of the exact structure and the resulting structure property relationship of the InGaAs heterostructure based on previously measured low-temperature photoluminescence spectra.[1]. As the functionality of these heterostructures, like efficient carrier confinement, is closely linked to their 3D structure and chemical composition, tomographic reconstructions employing STEM HAADF tilt-series were carried out. To this end a tilt series with a tilt range from -75° to 75° was measured on a probe corrected FEI Titan Themis electron microscope and reconstructed using a weighted SIRT algorithm as well as finite support correction after preprocessing and alignment. The resulting tomogram is shown as an isosurface in Figure 1a. It consists of six sidewall facets perpendicular to the main [111] growth direction terminating in aflat capping layer. Assuming Lambert-Beer's law, the obtained attenuation coefficients can be qualitatively correlated to atomic numbers by using two reference areas of the tomogram, here AlGaAs (Al and Ga assumed to be 1:1) and GaAs neglecting the very low Sb concentration. As the Z-contrast shows the average atomic number of the elements present, AlGaAs was set to Z = 27.5 and GaAs set to Z = 32 respectively. This assumes the small differences in crystal parameters between AlGaAs and GaAs are neglectable. The resulting element mapping corresponds well with the elemental compositions obtained from EDX, as can be seen by comparing Figure 1b and the corresponding EDX data acquired in the same projection direction in Figure 1c. While the facets are well measured some missing wedge artifacts and a slight density gradient based on the unaccounted carbon support are still present as seen in the slices along the growth direction shown in Figure 1e. The threefold faceted capping layers as seen in Figure 1e(i) show a truncated tetrahedral growth governed by the threefold symmetry of the ZnS type crystal structure of GaAs in combination with twinning defects. In order to validate the use of the Lambert-Beer-Law for STEM HAADF measurements, pytorch multi-slice simulations were conducted for GaAs at different tilt angles using the frozen phonon approximation to account for thermal diffuse scattering, and compared to the experimental results. Furthermore, the possibility to reducing the artifacts resulting from the missing wedge focus series are investigated by multi-slice simulations and experiments.

Figure 1: STEM tomographic analysis of the GaAsSb/InGaAs/AlGaAs NW heterostructure; (a) 3D isosurface rendering of the NW tip, illustrating the facet structure consisting of six sidewall facets perpendicular to the [111] growth direction. (b) Z-contrast volume rendering of the NW, (c) corresponding EDXS map of the same NW with comparable color code, (d) two central cuts parallel to {1-10} sidewall facets (as indicated in (a)), exposing the Z-contrast through the core. (e) Cross-sections at different positions along the NW (as indicated in (d) by labels (i)-(iv)), revealing the Z-contrast in radial direction from top (GaAs) to bottom (GaAsSb) of the NW heterostructure.

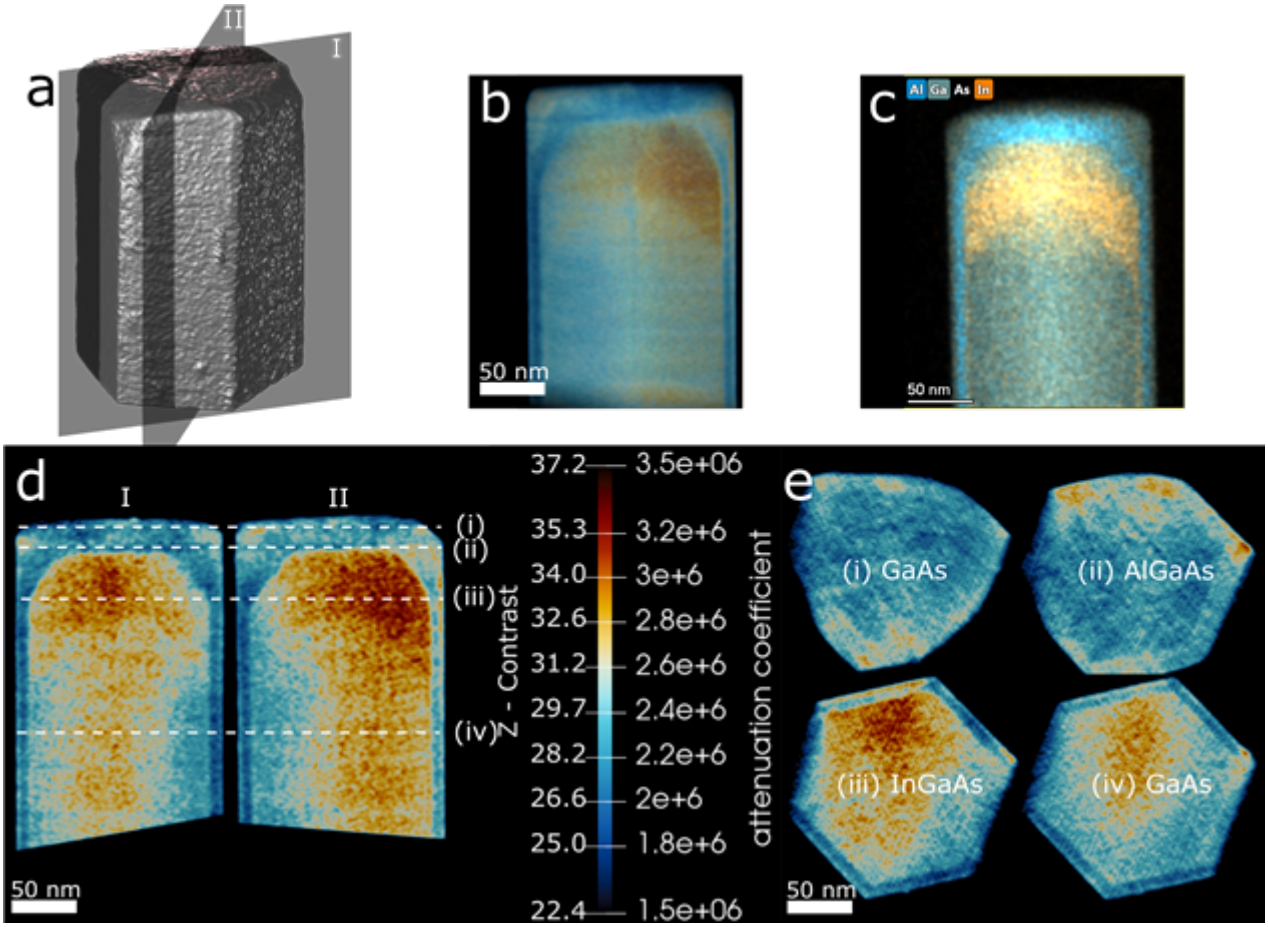

Keywords:

Nanowires, Tomography, STEM, Simulations, GaAs

Reference:

1. H. W. Jeong, ACS Appl. Nano Mater. 2024, 7, 3, 3032–3041
2. G. Koblmüller; B. Mayer; T. Stettner; G. Abstreiter; J. J. Finley; invited review. Semicond. Sci. Technol. 2017, 32 (5), 053001.
3. S. Kim, Nat. Photonics 2009, 3 (10), 569–576

1098

In-Situ microscopy study on self-healing process of vitrimers

Tobias Krekeler[1], Siraphat Weerathaworn[2], Matthias Hemmleb[3], Volker Abetz[2], Martin Ritter[1]
[1]Hamburg University of Technology, Hamburg, Germany, [2]University of Hamburg, Hamburg, Germany, [3]point electronic GmbH, Halle (Saale), Germany

Poster Group 1

Vitrimers are reprocessable and recyclable polymers with a wide range of adjustable properties. One keypoint of the reprocessability is the thermoreversible associative dynamic exchange mechanism which makes a vitrimer behave like viscoelastic fluid at elevated temperatures and like a thermoset at low temperatures. This change in behavior also has the potential to design polymers with "self-healing" characteristics where scratches or fractures are removed by applying heat. In this work we track this self-healing mechanism of a scratched vitrimer surface with in-situ microscopy and surface reconstruction using a segmented backscatter electron detector. The vitrimer used in this study is a tailor-made vinylogous urethane vitrimer with self-assembling binary and ternary block and random copolymers.[1]
The surface height of the sample is obtained with a shape-from-shading algorithm that uses the angular dependency of backscattered electrons and the orientation of the surface inclination to the detector. This technique does not need sample tilting and allows for live in situ topographic view of sample surfaces.[2]
The topographic view of the scratch show the displaced material as a 2 µm high ridge on both sides right next to the 5 µm deep scratch. After heating the sample to 115 °C for 2 minutes the ridges have flattened to a large extent due to the transition of the polymer to a fluidic state.
This initial result show the great potential of topographic imaging in in-situ experiments as conventional SEM imaging only result in 2D-images without or only obfuscated height information.

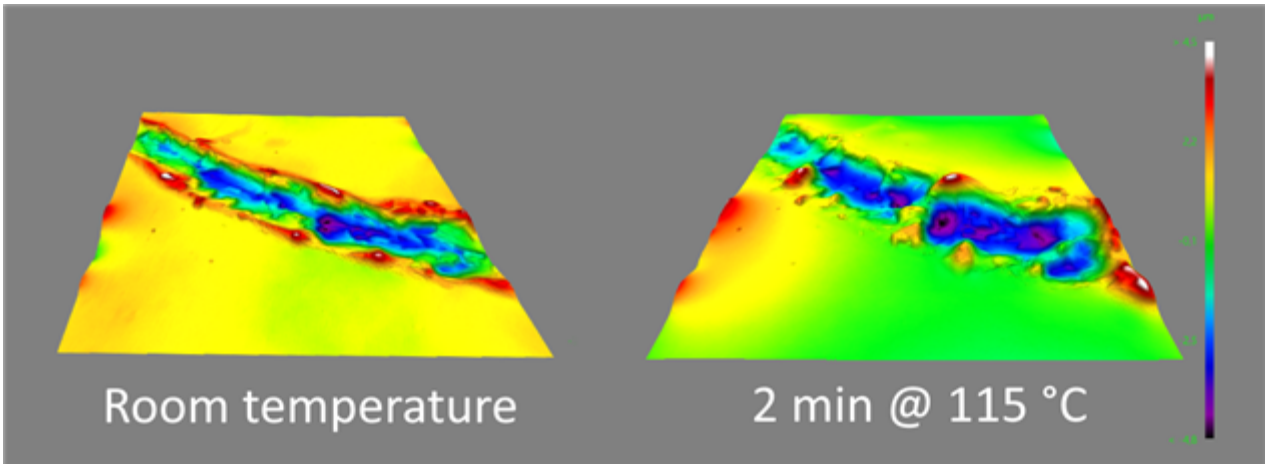

Keywords:

shape-from-shading, in-situ microscopy, vitrimers

Reference:

[1] S. Weerathaworn, V. Abetz “Tailor-Made Vinylogous Urethane Vitrimers Based on Binary and Ternary
Block and Random Copolymers: An Approach toward Reprocessable Materials.” Macromol. Chem. Phys. 2023,
224, 2200248.

[2] M. Hemmleb, D. Bettge, I. Driehorst, D. Berger: “3D surface reconstruction with segmented BSE detector: New improvements and application for fracture analysis in SEM”. EMC 2016, pp. 489-490. DOI: 10.1002/EMC2016.0709

1140

Visualisation of lepidopteran silk gland morphology using X-ray micro-computed tomography scanning technique

Mgr. Šárka Podlahová[1,2], Mgr., Ph.D. Gabriela Krejčová[1], Mgr., Ph.D. Hana Sehadová[1,2]
[1]University of South Bohemia in České Budějovice, Faculty of Science, České Budějovice, Czech Republic, [2]Biology Centre of the Czech Academy of Sciences, Institute of Entomology, Ceske Budejovice, Czech Republic

Poster Group 1

Background incl. aims
Lepidopteran caterpillars are one of the most significant insect silk producers. Depending on diverse life strategies of the two sister families of Bombycoidea, Saturniidae and Sphingidae, the caterpillars have evolved various ways of using silk. Most of the sphingiid larvae use silk exclusively in their first instars to produce rescue silk fibres that prevent the tiny caterpillars from falling off the host plant. In contrast, their closest relatives, the Saturniidae, save all of their silk for the end of larval development to construct complex silk cocoons that serve as a protective outer shell for the individual during its pupal stage. In general, silk is secreted by specialised ectodermal cells that form a silk gland. The silk glands of individual lepidopteran families differ significantly in their overall morphology. This research aims to analyse the in situ localisation of silk glands of several representatives of the Saturniidae and Sphingidae using micro-computed tomography (microCT). The data obtained allow the generation of detailed 3D projections of a caterpillar body, including its internal organs. Here we compare the advantages of the Surface module for segmentation and surface rendering in three different versions of the Imaris software (Imaris 9.3, Imaris 10.0 and Imaris 10.1).
Methods
Last instar caterpillars of the Saturniidae and Sphingidae representatives were submerged in Bouin-Hollande's fixative and contrasted in Lugol's solution. X-ray microCT SkyScan, model 1272 (Bruker microCT, Belgium) was used to visualise iodine-contrasted specimens. High-resolution 3D output tomography data were reconstructed in SkyScan’s volumetric NRecon software version 2.2.0.6 (Bruker microCT, Belgium). 3D models were created in Imaris software versions 9.3, 10.0 and 10.1 (Bitplane AG, Oxford Instruments, UK) using the Surface module: Surpass - Contour Surface, and Machine learning segmentation based on Artificial Intelligence.
Results
Non-invasive microCT is the ideal technology to project internal structures and organs in situ without destroying the specimens. Using Imaris analysis software, we found that Imaris 9.3 is excellent at creating semi-transparent surfaces with adjustable transparency, while the latest Imaris 10.1 does not allow this. On the other hand, Imaris 10.1 uses Machine learning segmentation based on Artificial Intelligence, which makes surface creation much faster and easier.
Conclusions
The procedure for preparing caterpillars for microCT has been optimised. Detection of silk glands in members of the Saturniidae and Sphingidae families based on microCT scanning reveals their exact location in the larval body. This approach allows detailed comparison of the silk gland morphology in relation to the location of other internal organs. Imaris 9.3 and Imaris 10.1 are a suitable combination for complex 3D renderings of biological objects.

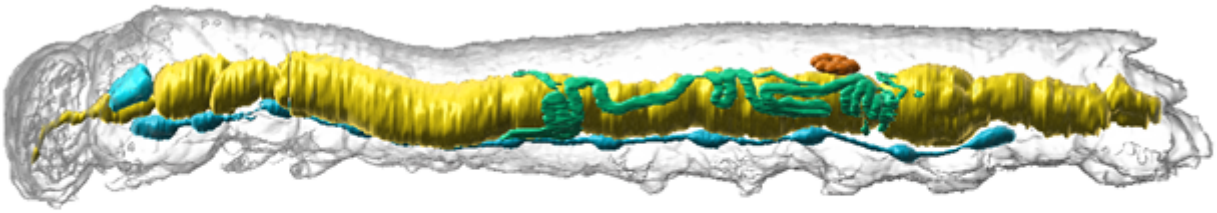

Keywords:

microCT, silk glands, Imaris

Reference:

Fedič, R., Žurovec, M., Sehnal, F. The silk of Lepidoptera. J. Insect Biotechnol. Sericol. 71: 1–15 (2002).
Schoborg, T.A. Whole Animal Imaging of Drosophila melanogaster using Microcomputed Tomography. J. Vis. Exp. (163), e61515 (2020).
Sehnal, F. and Akai, H. Insects silk glands: their types, development and function, and effects of environmental factors and morphogenetic hormones on them. Int. J. Insect Morphol. Embryol. 19, 79-132 (1990).